Renewable Energy 199 (2022) 1606–1628

Contents lists available at ScienceDirect

Renewable Energy

journal homepage: www.elsevier.com/locate/renene

The potential of transcritical cycles based on CO_2 mixtures: An exergy-based analysis

Pablo Rodríguez-deArriba, Francesco Crespi *, David Sánchez, Antonio Muñoz, Tomás Sánchez

Department of Energy Engineering, University of Seville, Camino de los descubrimientos s/n, 41092 Seville, Spain

ARTICLE INFO

Keywords:
CO_2 cycles
CSP applications
CO_2-blends
Exergy analysis

ABSTRACT

This paper focuses on the thermodynamic comparison between pure supercritical Carbon Dioxide and blended transcritical Carbon Dioxide power cycles by means of a thorough exergy analysis, considering exergy efficiency, exergy destruction and efficiency losses from Carnot cycle as main figures of merit. A reference power plant based on a steam Rankine cycle and representative of the state-of-the-art (SoA) of Concentrated Solar Power (CSP) plants is selected as base-case. Two different temperatures of the energy (heat) source are considered: 575 °C (SoA) and 725 °C (next generation CSP).

Compared to SoA Rankine cycles, CO_2 blends enable cycle exergy efficiency gains up to 2.7 percentage points at 575 °C. At 725 °C, they outperform both SoA and pure CO_2 cycles with exergy efficiencies up to 75.3%. This performance is brought by a significant reduction in the exergy destruction across the compression and heat rejection process rounding 50%. Additionally, it has been found that the internal condensation occurring inside the heat recuperator for those mixtures with a large temperature glide improves recuperator exergy efficiency, supporting the use of simpler layouts without split-compression. Finally, CO_2 blends exhibit lower cycle exergy efficiency degradation than pure sCO_2 in the event of an increase in the design ambient temperature.

1. Introduction

Concentrated Solar Power (CSP) is widely considered as a very promising contributor towards a complete carbon-free power generation scenario, due to its renewable nature and high dispatchability when coupled with thermal energy storage (TES). However, further investigation is mandatory to reduce CSP levelised cost of electricity (LCoE) in order to make this technology competitive in the energy market. The solar subsystem, composed by solar field, receiver and tower, undoubtedly represents the main contributor to the Overnight Capital Cost (OCC) of Solar Tower technology (ST), closely followed by the TES [1]. Thus, increasing CSP overall performance results to be a mandatory step in the pathway to achieve a reductions in size and cost of these components. Recent studies confirm that the greatest room of improvement lies in the power block, indicating as possible solution the adoption of innovative power cycles, capable of achieving thermal efficiency significantly higher than the one obtained by the state-of-the-art steam-based Rankine [2,3]. In this regard, the potential of supercritical carbon dioxide (sCO_2) power cycles has already been recognised by the CSP industry [3] and extensively investigated in the last decade [1,4–8], due to several beneficial aspects inherently enabled by sCO_2 technology: firstly, a significant reduction in the compression work, achieved by performing compression near the critical point, where the specific volume significantly drops due to real-gas effects (see Fig. 2 in [9]); secondly, the outstanding thermal stability of CO_2, which theoretically enables turbine inlet temperature equal or higher rounding 700 °C [10], a value widely recognised as a threshold for next-generation solar towers plants and significantly higher than the SoA one (550 °C). As a matter of fact, several studies confirm the possibility to achieve power block efficiency equal or higher than 50%, employing sCO_2 cycles with a turbine inlet temperature rounding 700 °C and a minimum cycle temperature in the order of 32–35 °C, a value extremely close to the critical point of carbon dioxide (T_{cr}=31 °C) [4]. sCO_2 technology has been extensively investigated in recent years, and very comprehensive research works can be found in the literature. Should the reader be interested in learning more about these and other aspects of this technology, the authors highly recommend the following readings: the seminal works of Angelino [11–13] and Feher [14], lately revived by Dostal [15], establishing the

* Corresponding author.
E-mail addresses: prdearriba@us.es (P. Rodríguez-deArriba), crespi@us.es (F. Crespi), ds@us.es (D. Sánchez), ambl@us.es (A. Muñoz), tmsl@us.es (T. Sánchez).

https://doi.org/10.1016/j.renene.2022.09.041
Received 17 February 2022; Received in revised form 7 September 2022; Accepted 10 September 2022
Available online 15 September 2022

Nomenclature

Acronyms

C_6F_6	Hexafluorobenzene
CSP	Concentrated Solar Power
D1	CO_2–C_6F_6 mixture
D2	CO_2–$TiCl_4$ mixture
D3	CO_2–SO_2 mixture
E_D	Exergy destruction [MW]
E_F	Fuel exergy [MW]
E_L	Exergy losses [MW]
E_P	Product exergy [MW]
ER_T	Turbine Expansion Ratio [–]
HRU	Heat Rejection Unit
HTRec	High Temperature Heat Recuperator
LTRec	Low Temperature Heat Recuperator
MW	Molecular Weight [g/mol]
OCC	Overnight Capital Cost
P_{max}	Maximum Cycle Pressure [bar]
PC	Partial Cooling cycle
PHX	Primary Heat Exchanger
pp	percentage point
PR_{MC}	Main Compressor Pressure Ratio [–]
PR_{Prc}	Precompressor Pressure Ratio [–]
PrC	Precompression cycle
RC	Recompression cycle
Rec	Heat Recuperator
RR	Recuperated Rankine cycle
sCO_2	Supercritical Carbon Dioxide
SO_2	Sulfur Dioxide
SoA	State-of-the-art
T_{min}	Minimum Cycle Temperature [°C]
$TiCl_4$	Titanium Tetrachloride
TIT	Turbine Inlet Temperature [°C]
W_s	Specific work [kJ/kg]

Greek symbols

α	Split-flow factor [–]
$\Delta\eta$	Efficiency losses from Carnot Cycle [%]
ΔP	Pressure drops [%]
ΔT_{min}	Recuperator Minimum Temperature Difference [°C]
ΔT_{PHX}	Temperature Rise in PHX [°C]
ϵ	Exergy efficiency [%]
η	Efficiency [%]

Subscripts

cond	condensation
cr	critical
cyc	cycle
is	isentropic
k	component
th	thermal

thermodynamic fundamentals of sCO_2; a thorough overview and categorisation of the different cycle configurations proposed in literature, provided by Crespi et al. [16], and a detailed description of the current state of the technology, presented by Brun et al. [17] and White et al. [9]; finally, cost estimates based on vendor quotes, specific for sCO_2 technology, can be found in the works of Carlson et al. [18] and Weiland et al. [19].

According to Turchi et al. [20], CSP tower plants currently in construction have an overnight capital cost in the range of 3300–6200 $/kW, depending on TES capacity (6 h and 13 h respectively). Furthermore, it is worth highlighting that the cost of various subsystems are expected to decrease in the upcoming years. In particular, estimations made in the framework of the SunShot Programme [21] foresee a reduction in the solar field cost from 140$/m^2 to 50–70$/m^2, in the site preparation cost from 16$/m^2 to 10$/m^2, in the tower and receiver cost from 137$/kW$_{th}$ to 100–120$/kW$_{th}$ and in the thermal storage cost from 22$/kWh$_{th}$ to 10–15$/kWh$_{th}$ (based on commercial Solar Salt). Nonetheless, this cost reduction seems not to be sufficient – not even in the most optimistic scenario – to achieve the target LCoE, currently set at 50$/MWh for conventional steam turbines [22]. As previously commented, higher power block efficiency would enable a significant reduction in the size and, expectedly, the cost of both solar field and thermal energy storage. However, it is worth remarking that higher TIT level also entails the need for advanced materials as well as a new technology for the Thermal Energy Storage (commercial Solar Salt cannot exceed 575 °C). As a consequence, the specific cost of the TES is prone to rise. Furthermore, supercritical CO_2 cycles have been proven to lead to a reduction in temperature difference across the solar receiver with respect to steam-based Rankine [6]. This also leads to an increase in the specific costs of TES, brought by the higher volume of salts required for the same amount of stored energy. As a consequence, techno-economic assessments for sCO_2 technology found in literature still provide unsatisfactory results when compared to SoA CSP, exacerbating the need for further investigation. Amongst others, Thanganadar et al. [8] concluded that OCC for sCO_2 significantly increases when TIT moves from 600 °C to 700 °C due to the negative impact on TES cost and, even in the former case, the calculated OCC rounds 5000$/kW (10 h TES), a value comparable to that of SoA Rankine; Crespi et al. estimated an OCC in the order of 5900 $/kW and 6870 $/kW for a *Partial Cooling* and *Recompression* cycle respectively (considering a 10 h TES capacity in both cases) [1]; finally, Alfani et al. obtained an OCC rounding 6630 $/kW for a *Recompression with Intercooling* cycle (15 h TES) [23]. Furthermore, the high ambient temperatures, a characteristic feature of CSP typical locations, are extremely detrimental for sCO_2 technology, since the compression process is shifted away from the vicinities of the critical point, compromising its actual potential in terms of thermodynamic gains against SoA Rankine. As a matter of fact, the drop in thermal efficiency can be as high as 4 percentage points (pp) when minimum cycle temperature (T_{min}) moves from 35 °C (close to critical point) to 50 °C (realistic value for CSP typical locations), independently on the cycle layout considered [24].

In order to overcome this weakness whilst still retaining the thermodynamic features enabling potentially higher efficiencies, the use of blended sCO_2 has been investigated in the very last years. Invernizzi & van der Stelt studied totally supercritical and condensation cycles of CO_2 mixed with benzene [25]. Later, Invernizzi extended his work to other hydrocarbons, such as toluene [26]. Baik & Lee provided experimental data of the performance of CO_2-R32 mixture, concluding that blended CO_2 working fluids can reduce the efficiency degradation of pure sCO_2 power cycles in warm environments [27]. Manzolini et al. performed a techno-economic assessment of CO_2 mixtures with $TiCl_4$ and N_2O_4 as dopants for Concentrated Solar Power applications and estimated a LCoE reduction of 10% in comparison with steam Rankine [28]. Valencia-Chapi et al. explored multiple CO_2 mixtures for Solar Power Plants applications, achieving an increase in thermal efficiency of 3–4 pp with respect to pure sCO_2 [29,30]. It is exactly in this scenario where the SCARABEUS project [31] is being developed, with the main idea of increasing the critical temperature of the working fluid through the addition of certain additives to the raw sCO_2, enabling its condensation even at very high ambient temperatures, thus producing

higher thermal efficiency than with either (steam) Rankine or sCO_2 cycles.

Thermal efficiency is a suitable figure of merit to compare power cycles working under similar heat source and sink temperatures. Nevertheless, the comparison between steam Rankine cycles and supercritical CO_2 cycles is often misleading because different turbine inlet temperatures (TIT) are involved: lower for steam cycles and higher for sCO_2 systems. In other words, higher energy efficiencies of the latter cycles can potentially be brought about by the higher temperatures of heat addition to the cycle and not by an inherently more efficient conversion of this energy into useful work. The utilisation of the 2nd Law of Thermodynamics to carry out an exergy analysis, as opposed to the more usual energy analysis, has a twofold benefit. On the one hand, it provides meaningful information about whether or not a cycle is closer to the best thermodynamic performance attainable for given heat source/sink temperatures (Carnot cycle). On the other, it allows the identification of those component where exergy losses are taking place; i.e., where cycle performance is departing from the ideal (reference) Carnot cycle. As a result, it is possible to modify the cycle layout to compensate for these losses, thus yielding a cycle performance closer to the true potential enabled by the temperatures of heat source and sink.

Several authors have carried out exergy analyses of sCO_2 cycles in the past [12,13,32,33], yielding the known conclusion that the main source of irreversibilities in the *Simple Recuperated* cycle operating on sCO_2 is the recuperative heat exchanger, due to the dissimilar heat capacity of the high- and low- pressure streams. This conclusion brought about a series of advanced layouts proposed by Angelino [12], featuring split-compression that resulted in the well-known *Recompression* and *Partial Cooling* layouts. These cycles largely improved the exergy efficiency of the *Simple Recuperated Brayton* cycle, redistributing exergy destruction and reducing the losses associated to the recuperative heat exchangers and the heat rejection unit, at the expense of increasing the losses across the compression and expansion processes. Such advanced sCO_2 cycles exhibit a more uniform loss distribution across the different cycle components, in contrast with that of the steam Rankine cycle which concentrates most of the exergy destruction in the primary heat addition process [13].

These conclusions about the most interesting cycle layouts for given boundary conditions can nevertheless change when the characteristics of the working fluid vary. Such is the case of the SCARABEUS project where the addition of additives brings about modifications of the working fluid properties (most notably the critical pressure and temperature). Previous studies, developed in the context of SCARABEUS by some of the authors, demonstrated that part-flow configurations can be of little interest for some sCO_2-based blends, due to poor adaptability to compression in liquid phase [24,34]. This is numerically confirmed for two of the additives currently under investigation in SCARABEUS – Hexafluorobenzene (C_6F_6) and Titanium Tetrachloride ($TiCl_4$) – and paves the way for the exploration of other cycle layouts. Amongst these, attention was paid by the authors to other cycle configurations that had been disregarded by the sCO_2 scientific community in the last years, in particular the *Recuperated Rankine* and *Precompression* cycles about which, unfortunately, only a few studies analysing the 2nd Law characteristics can be found in literature. On the contrary, the *Recompression* cycle does exhibit a good performance for the third additive hereby studied, Sulfur Dioxide (SO_2), due to a much narrower Pressure–Temperature envelope of the resulting mixture, inherently brought by the use of this dopant [35].

Bearing all this in mind, the present paper aims to analyse the intrinsic 2nd Law performance of sCO_2 cycles in depth, following the footsteps of Gianfranco Angelino back in the late 1960s, with the aim of exploring the performance enhancement that sCO_2 blends could potentially bring to the technology. To this end, two different heat source temperatures are considered: 575 °C, representative of contemporary CSP plants using state-of-the-art technology, and 725 °C, representative of next-generation receiver technologies. The work is organised as follows: In the first part of the manuscript a thorough description of the computational environment is provided, followed by a brief introduction to the fundamentals of exergy analysis as used in the paper. In the second part, sCO_2 cycles, either pure or blended, are optimised and compared between them and against SoA CSP Rankine cycles using steam, and a series of interesting conclusions are drawn. Afterwards, a parametric analysis of the two key optimisation variables – maximum cycle pressure (P_{max}) and molar composition of the working fluid – is conducted. Finally, the effects of varying minimum cycle temperature are investigated by means of a sensitivity analysis, comparing both pure and blended CO_2-based systems.

Table 1
Common set of boundary conditions for sCO_2-based cycles (pure or blended).

Parameter	Value
Maximum cycle pressure [bar]	250
Minimum cycle temperature [°C]	50
Turbine inlet temperature [°C]	550/700
Turbine isentropic efficiency [%]	93
Compressor isentropic efficiency [%]	89
Pump isentropic efficiency [%]	88
Heat exchangers temperature approach [°C]	5
Primary heat exchanger pressure drops [%]	1.5
Heat rejection unit pressure drops [%]	1.0
Heat recuperator pressure drops [%]	1.0 (low pressure side) 1.5 (high pressure side)

2. Computational environment

2.1. Definition of reference case, candidate cycles and blends

Three different power cycle technologies are considered in this work: (i) SoA steam-based Rankine cycles, (ii) pure supercritical CO_2 cycles and (iii) transcritical cycles using CO_2 blends. Due to the intrinsic differences between these technologies, in particular between the Rankine and sCO_2-based cycles (either pure or blended), it is not possible to define a complete set of common boundary conditions to be employed in the simulations. Rather, the only common specifications are power output, set to 100 MW gross, minimum cycle temperature, set to 50 °C to have a representative value applicable to a site with extreme ambient conditions, and the two heat source temperatures, 575 and 725 °C respectively.

The reference power cycle considered for contemporary CSP plants using steam turbine technology features reheat and feedwater heating. Live steam is produced at 150 bar and 550 °C and the extraction pressures for the seven feedwater heaters are set so as to balance peak cycle efficiency and inventory and auxiliary power consumption of the molten salt system. Condensation is enabled by an Air-Cooled Condenser with a design pressure of 0.123 bar (50 °C).[1]

For the cycles based on CO_2, either pure or blended, a total of five different cycles are considered: *Recuperated Rankine*, *Precompression* and *Recompression* for CO_2 mixtures, *Recompression* and *Partial Cooling* for pure sCO_2. These cycle configurations were originally proposed by Angelino in 1968 [12] and their layouts are shown in Fig. 1, along with the corresponding temperature–entropy diagrams. The first cycle is a mere adaption of a Rankine cycle employing CO_2-based blends, whilst the remaining ones are characterised by advanced layouts, originally proposed to enhance the performance of the simple recuperative by

[1] This power block is adapted from the cycle proposed for the Rice Solar Energy Project in California [36]. When the higher heat source temperature is taken into account (725 °C), live steam is produced at 180 bar and 600 °C, herein considered as the maximum live steam temperature enabled by SoA steam turbine technology.

Table 2
Thermodynamic properties of dopants.

	MW [kg/kmol]	T_{cr} [°C]	P_{cr} [bar]	Thermal stability
CO_2	44.01	31.06	73.83	>700 °C [10]
SO_2	64.06	157.60	78.84	>700 °C [10]
C_6F_6	186.06	243.58	32.73	up to 625 °C[a]
$TiCl_4$	189.69	364.85	46.61	up to 700 °C[a]

[a]Threshold temperature currently obtained by University of Brescia and Politecnico di Milano for the SCARABEUS project. Complete set of experimental results to be disclosed in an oncoming publication by these two institutions.

Table 3
Additive hazard according to NFPA 704 [37].

Compound	Health hazard	Flammability	Chemical reactivity	Special hazard
CO_2	2	0	0	Simple Asphyxiant
C_6F_6	1	3	0	–
$TiCl_4$	3	0	2	React with water
SO_2	3	0	0	–

means of two different approaches. On the one hand, the *Precompression* layout is characterised by the addition of a pre-compressor in the low-pressure section of the cycle, between the high and low temperature recuperators, in order to overcome the limitation imposed by condensing pressure on turbine exhaust pressure. This provides an additional degree of freedom for further optimisation, increasing the expansion ratio achievable by the turbine. On the other hand, the *Recompression* cycle is obtained by dividing the flow of working fluid in two different streams before the heat rejection unit: one is sent to HRU, main compressor (or pump, in transcritical embodiment) and the low temperature recuperator (LTRec), whilst the other is compressed in a re-compressor and mixed with the former stream at LTRec outlet. The final aim of this stratagem, as claimed by Angelino, is to enhance LTRec heat recuperation potential by decreasing the internal irreversibilities of this components, by means of a reduction of the mass flow circulating through the high-pressure/low-temperature side of LTRec. The latter, in fact, is usually characterised by a really high mean specific heat due to the vicinity to the critical point, and a drop in its mass flow is found to be a very effective means to balance the heat capacities of the two sides of the recuperator, improving the exergy efficiency of this heat exchanger. Finally, the *Partial Cooling* cycle is an evolution of the *Recompression*, obtained by adding a heat rejection unit and a compressor before the split-flow. Thanks to this particular configuration, the *Partial Cooling* cycle ensures a very good compromise between thermal efficiency, specific work and temperature rise across primary heat exchanger, standing as one of the most promising alternative for CSP plant applications [1].

A common set of boundary conditions applied to all CO_2-based systems is summarised in Table 1, where two Turbine Inlet Temperatures (TIT) are considered, 550 °C and 700 °C, corresponding to the two different heat source temperatures mentioned above. In the first step of the analysis, the maximum cycle pressure and the minimum cycle temperature are set to 250 bar and 50 °C respectively, and the influence of the variations of these parameters is then study at the end of this manuscript by means of sensitivity analysis. In spite of fixing a set of common boundary conditions, it is worth remarking that each different cycle presents a series of specific parameters (i.e. degrees of freedom) that can be varied in order to maximise its thermal efficiency. Considering pure CO_2 systems, the main compressor pressure ratio (PR_{MC}) can be optimised, for a given maximum cycle pressure, varying the pressure level at compressor inlet (station 1 in both cycle configurations, see Fig. 1a and b). This allows to achieve a compromise between the beneficial and detrimental effects of compressing near the critical point (reduction in compression work, increase in irreversibilities in the heat regeneration). On the contrary, pump inlet pressure is not a degree of freedom in SCARABEUS systems and, for a given blend, cannot be modified without affecting the minimum cycle temperature, due to the condensing nature of these cycles. On the other hand, optimising the molar fraction of dopant – varying the composition of the working fluid and, thus, shifting the critical point itself – results to be a very interesting mean to increase both thermal and exergy efficiency of SCARABEUS systems. Furthermore, the turbine expansion ratio (ER_T) can be freely optimised in the *Partial Cooling* and *Precompression* cycles, independently on the PR_{MC}, varying the pressure ratio of the precompressor (PR_{PrC}, stations 10–11 and 7–8 for *Partial Cooling* and *Precompression* respectively, see Fig. 1b and d). Finally, the split-flow factor α, defined as the percentage of the working fluid circulating through the recompressor and low-temperature recuperator, is a very interesting optimisation parameter for *Recompression* and *Partial Cooling* cycles (stations 1, 2 and 3 for both configurations). The optimum values of all these parameters are further discussed in Section 4.1 and disclosed in Table 6.

The main thermodynamic characteristics of the three candidate dopants are provided in Table 2, whilst a brief evaluation of these additives is summarised in Table 3, following NFPA 704 standard. For sake of comparison, the same parameters referring to Carbon Dioxide are added in both tables. Some of these features are currently under evaluation by the SCARABEUS consortium in order to assess how much they compromise the commercial deployment of the technology (high flammability of C_6F_6, aggressive water reactivity for $TiCl_4$ and toxicity of SO_2). In particular, it is worth mentioning that the preliminary results obtained by SCARABEUS consortium found that C_6F_6 is expected to present a thermal stability significantly lower than the other chemical compounds in analysis and, more importantly, lower than the TIT level considered as representative for next-generation CSP plant. In spite of this fact, authors decided to investigate the performance of CO_2-C_6F_6 blends for the entire set of boundary conditions employed in the present paper, in order to provide a complete comparison with the other dopants in analysis. Nevertheless, if the threshold temperature indicated in Table 2 will be confirmed, this would be a crucial limitation to the adoption of CO_2-C_6F_6 mixtures in high-temperature CSP applications. Further information about this and other dopants being screened now will be reported by the corresponding partners in future publications.

The thermodynamic properties of the CO_2-based mixtures have been obtained with the commercial software Aspen Plus [38] (more information can be found in previous works by the authors [24,35]). The critical loci, the pressure–temperature envelopes and the main thermodynamic properties of the three sCO_2 mixtures considered in this work are provided in Fig. 2 and Table 4.

2.2. Simulation tools

The modelling and simulation of the power cycle has been developed using the commercial software Thermoflex [39], a widely used software for power plant engineering and analysis with built-in data sets of steam and carbon dioxide properties using Refprop database [40]. Unfortunately, Thermoflex does not have a similar database of properties for CO_2 mixtures of variable composition. These

Table 4
Main characteristics of working fluids. P_{cond} and temperature glide refer to a bubble temperature of 50 °C.

Mixture	Molar comp. [%]	MW [kg/kmol]	T_{cr} [°C]	P_{cr} [bar]	P_{cond} [bar]	Glide [°C]
D1C15	CO_2–C_6F_6 [85–15]	65.32	102.1	121.3	77.52	88.4
D2C17	CO_2–$TiCl_4$ [83–17]	68.77	116.4	212.6	96.17	181.6
D3C20	CO_2–SO_2 [80–20]	48.03	64.2	91.85	77.41	16.1

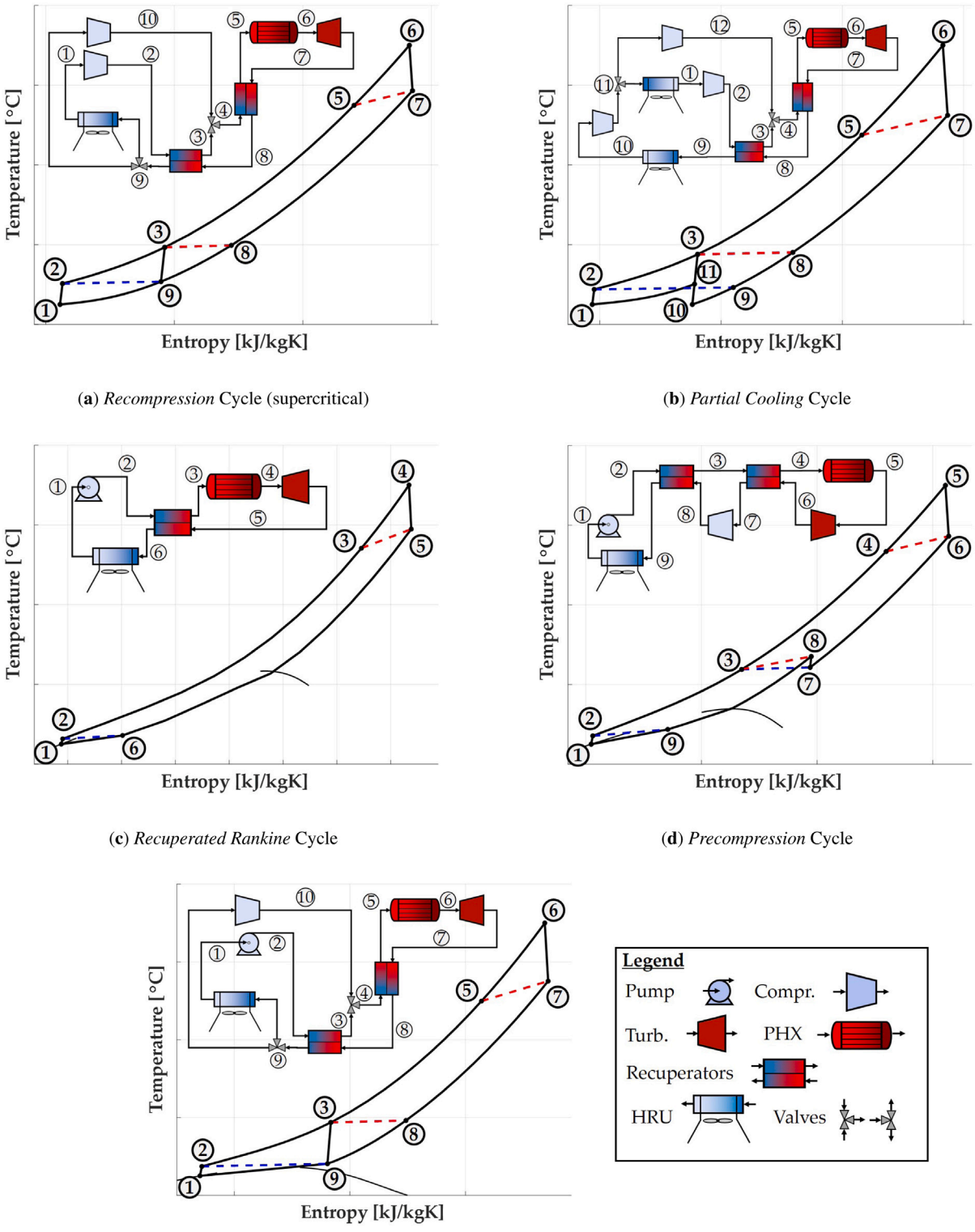

(**a**) *Recompression* Cycle (supercritical)

(**b**) *Partial Cooling* Cycle

(**c**) *Recuperated Rankine* Cycle

(**d**) *Precompression* Cycle

(**e**) *Recompression* Cycle (transcritical)

Fig. 1. Cycle layouts considered for pure (a, b) and blended (c, d, e) CO_2 systems.

properties have thus been estimated with Aspen Plus [38] and the resulting data has been incorporated into Thermoflex through a dedicated User-defined General Fluid feature specifically developed by Thermoflow for the SCARABEUS project. Further information regarding the calculation of thermophysical properties can be found in previous papers by the authors [24,35] and by other partners of the SCARABEUS consortium [41]. The models in Thermoflex have been linked to an external optimiser in Matlab, using the *surrogateopt* function included in Matlab's 'Global Optimisation Toolbox'. Finally, several in-house Matlab code have been developed to obtain the exergy analysis from the

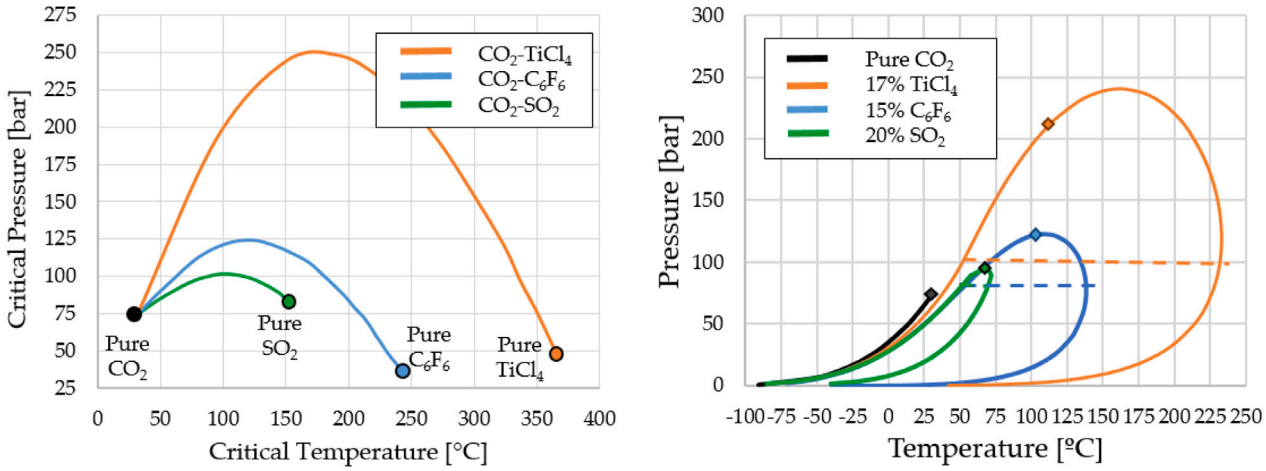

(**a**) Critical loci (**b**) Pressure-Temperature envelopes

Fig. 2. Thermodynamic features of the candidate blends: Critical loci (a) and Pressure–Temperature envelopes (b) are provided.

Table 5
Definition of fuel exergy, product exergy and exergy losses for each component.

Component	E_F	E_P	E_L	Component	E_F	E_P	E_L
Pump	W	E2−E1	adiabatic	Compressor	W	E2−E1	adiabatic
Turbine	E1−E2	W	adiabatic	Recuperator	E3−E4	E2−E1	adiabatic
PHX	$Q(1-\frac{To}{T})$	E2−E1	adiabatic	HRU	E1−E2	0	$Q(1-\frac{To}{T})$
Mixer	E1 + E2	E3	adiabatic	Splitter	E1	E2+E3	adiabatic

Table 6
Cycle optimum specifications for all the CO_2-based configurations studied. Two energy source temperatures are considered (575/725 °C).

Acronym	Layout	Working fluid	PR_{MC}	ER_T	PR_{PrC}	α
RC CO_2	*Recompression*	100% CO_2	2.37/2.45	2.20/2.27	X	0.29/0.29
PC CO_2	*Partial Cooling*	100% CO_2	2.23/2.24	3.18/3.70	1.55/1.80	0.4/0.41
PrC D1	*Precompression*	85% CO_2/15% C_6F_6	3.22/3.22	3.91/4.20	1.31/1.41	X
RR D2	*Rec. Rankine*	83% CO_2/17% $TiCl_4$	2.60/2.60	2.47/2.47	X	X
RC D3	*Recompression*	80% CO_2/20% SO_2	3.16/3.16	2.93/2.93	X	0.38/0.38

heat and mass balances calculated in Thermoflex and to post-process the results.

3. Fundamentals of exergy analysis

Exergy can be defined as the maximum work that can be extracted from a thermodynamic system from its current state until a final state of equilibrium with the environment – the dead state – is reached, assuming that the system interacts with the environment only [42]. Flow exergy of the working fluid can be calculated using Eq. (1), where H_0 and S_0 are the enthalpy and entropy at the pressure and temperature of the environment P_0 and T_0, here set to 40 °C and 1 bar. Other forms of exergy such as kinetic, potential and chemical exergy have not been considered in the analysis, and the cycles are assumed to operate in steady-state.

$$E_{flow} = (H - H_0) - T_0(S - S_0) \quad (1)$$

The approach to exergy analysis employed in this work is inspired by the work by Penkuhn and Tsatsaronis [33]. Thermodynamic irreversibility is a consequence of the generation of entropy over a thermodynamic transformation, also called "exergy destruction" (E_D), and this can be applied to both the individual components (Eq. (2)) and overall power cycle (Eq. (3)); these are identified with the sub-index *k* and *cyc* respectively. Regarding heat rejection and addition, constant cold and hot reservoir temperatures are considered, set to 40 °C and 575/725 °C (depending on TIT) respectively. The definition of this parameter makes use of the concept of product exergy (E_P), fuel (or educt) exergy (E_F)[2] and Exergy losses (E_L), explained in detail

[2] Following the definition provided in [43], the authors have considered the fuel or educt exergy to be representative of *all* the resources expended to provide the product exergy, not only the one characterised by higher exergy. Despite the possible dual denomination (i.e. fuel or educt), the authors have decided to employ only the former in the remainder of the manuscript for the sake of simplicity.

in [43,44] Table 5 includes fuel exergy, product exergy and exergy losses definition for all the components considered in this work [45].

$$E_{D,k} = T_0 \Delta S_{gen,k} = E_{F,k} - E_{P,k} - E_{L,k} \quad (2)$$

$$E_{D,cyc} = E_{F,k} - E_{P,cyc} - E_{L,cyc} \quad (3)$$

In addition to these parameters, the following two figures of merits are added to the analysis: exergy efficiency (ϵ) and *Efficiency losses from Carnot Cycle* ($\Delta\eta_k$). The first index is well-known and defined as the ratio between product exergy and fuel exergy, applicable to both individual components (Eq. (4)) and global system (Eq. (5)). The second metric, though, deserves a more thorough explanation. $\Delta\eta_k$ is a means to translate the irreversibility taking place in each individual component (typical of 2nd Law analysis) into an actual thermal efficiency loss (1st Law), employing Carnot cycle efficiency as a reference case [46]. With this in mind, the thermal efficiency loss brought about by a component is defined as the ratio between the exergy destruction that takes place in that particular component and the heat provided to the cycle (Q_{in}). The correlation employed to calculate this parameter is provided in Eq. (6).

$$\epsilon_k = \frac{E_{P,k}}{E_{F,k}} = 1 - \frac{E_{D,k} + E_{L,k}}{E_{F,k}} \quad (4)$$

$$\epsilon_{cyc} = \frac{E_{P,cycle}}{E_{F,cycle}} = 1 - \frac{\sum_k (E_{D,k} + E_{L,k})}{E_{F,cyc}} \quad (5)$$

$$\Delta\eta_k = \frac{T_0 \Delta S_{gen,k}}{Q_{in}} \quad (6)$$

4. Results and discussion

In this section the complete set of results obtained with Thermoflex software are presented and discussed. Firstly, a justification of the optimum cycle configuration (e.g. layout synthesis) for each different dopant is provided from an exergy perspective, confirming the potential of SCARABEUS concept to reduce cycle internal irreversibilities. Secondly, the optimised blended cycles – *Precompression* with C_6F_6, *Recuperated Rankine* with $TiCl_4$ and *Recompression* with SO_2 – are compared against pure CO_2 technology and SoA Rankine cycle by means of a combined 1st and 2nd law analysis. Afterwards, a parametric analysing varying cycle maximum pressure, molar fraction of dopant and ambient temperature is undertaken, studying the dependence of exergy efficiency on these three parameters.

4.1. Optimum specification and layout synthesis for the CO_2-based power cycles

Before assessing the optimum cycle configurations for the different dopants taken into account in the present study, a preamble discussing the main implications of employing these novel working fluids results to be mandatory. CO_2-based mixtures can be studied under either supercritical (pressure and temperature of any cycle stations higher than the corresponding critical values) or transcritical embodiments (subcritical conditions at pump and/or HRU inlet). If a fully supercritical set-up is adopted, the main compressor inlet pressure can be optimised in order to maximise thermal efficiency, achieving the perfect compromise between the advantages and disadvantages of operating the compression near the critical point: on the one hand, a low compression work, brought by the low specific volume of the working fluid at those conditions; on the other hand, high exergy destruction in the recuperator, due to the vast increase in the heat capacity of the cold stream inside this component, which directly affects to cycle heat regeneration potential [13]. On the contrary, if transcritical embodiments are taken into account, pump inlet pressure cannot be freely optimised, since it is fixed by cycle minimum temperature (T_{min}) due to the condensing nature of the cycle. For a given dopant, the transition from supercritical to transcritical embodiment theoretically depends on the molar composition of the working fluid, since as long as the critical temperature of the mixture is below the minimum cycle temperature, the cycle remains supercritical. There exits, therefore, a value of dopant molar fraction at which the critical temperature equals T_{min}. As a consequence, if a suitable amount of dopant is added, condensation even at high ambient temperatures can be enabled. If a simple recuperative cycle is taken into account with a T_{min} set at 50 °C, this threshold value corresponds to 4% for C_6F_6, 7% for $TiCl_4$ and 12% for SO_2, as can be observed in Fig. 3. Whether or not this strategy (i.e., SCARABEUS concept) can actually bring about an enhancement of the thermodynamic performance of pure sCO_2 cycles will depend on the specific dopant selected, its molar content and the cycle layout employed. In this context, an exergy analysis can reveal how the irreversibilities within different cycle configurations are altered when C_6F_6, $TiCl_4$ or SO_2 are added to CO_2.

Fig. 3 shows the breakdown of exergy destruction as a function of dopant molar fraction, obtained considering the different components of a simple recuperative cycle – Turbine, Pump/Compressor, Primary Heat Exchanger (PHX), Heat Recuperator (Rec) and Heat Rejection Unit (HRU) – operated with the three CO_2-based mixtures considered in the present study. The transition from a supercritical embodiment (hereby called *Simple Recuperated*) to transcritical one (*Recuperated Rankine*) has been emphasised with a dashed line. A first observation is that an optimum composition capable of minimising the total exergy destruction (stack value of all five areas) can be identified, and it results to be in the order of 15%–20% for C_6F_6, and approximately 17% and 8% for $TiCl_4$ and SO_2 respectively. Interestingly, the optimum composition for the two first dopants lies inside the transcritical zone, achieving an important reduction (23.3% and 37%, respectively) in the total exergy destruction with respect to the reference CO_2 cycle (0% molar fraction of dopant); on the contrary, the lowest overall exergy destruction observed for SO_2 mixtures corresponds to a fully supercritical embodiment, and it results to be only 5% lower than the one obtained considering pure CO_2. This circumstance can be explained by comparing the exergy destruction breakdown of each dopant. It is observed that the adoption of transcritical configurations enables a significant reduction (>50%) of the exergy destroyed in the Heat Rejection Unit (HRU), independently on the dopant. This is an indirect consequence of the lower temperature rise produced by the compression process, brought by operating the latter in liquid phase [25], which reduces the duty of the HRU [24]. For the three cases, the exergy destroyed in the turbomachinery decreases with a rise in dopant molar fraction, mainly due to the increasing molar mass of the mixture [46]. On the contrary, the exergy destruction in the PHX (slightly) diminishes continuously with the molar fraction for C_6F_6 and $TiCl_4$, whilst it rises significantly when the molar fraction of SO_2 is increased. This indicates that the addition of C_6F_6 and $TiCl_4$ potentially reduces the heat duty of the PHX, thanks to a higher heat recuperation. As a consequence, it could be expected that the exergy destruction in the recuperator (grey area in Fig. 3) would increase for mixtures based on C_6F_6 or $TiCl_4$ and decrease for SO_2, accordingly to the higher and lower fuel exergy involved in this equipment. Nevertheless, when SO_2 is added to the raw CO_2, the use of a transcritical embodiment always produces a significant rise in the exergy destroyed in the recuperator ($E_{D,Rec}$) with respect to the pure CO_2 case, contrarily to what can be observed for C_6F_6 and $TiCl_4$. These circumstance can be explained taking a step back and focusing on the definition of exergy efficiency of a single equipment ϵ_k: according to Eq. (4), $E_{D,Rec}$ is equal to the product of the fuel exergy and (1-ϵ_{Rec}). In this regard, Fig. 4(a) depicts both fuel exergy and exergy efficiency of the recuperator as a function of the dopant molar fraction for the three candidate blends. As expected, the fuel exergy increases with the molar content of C_6F_6 and $TiCl_4$ and is reduced when adding SO_2. Whereas the exergy efficiency is inversely proportional to the molar fraction in the SO_2 case, there exists a minimum value for C_6F_6 and $TiCl_4$ from which the exergy efficiency of the recuperator

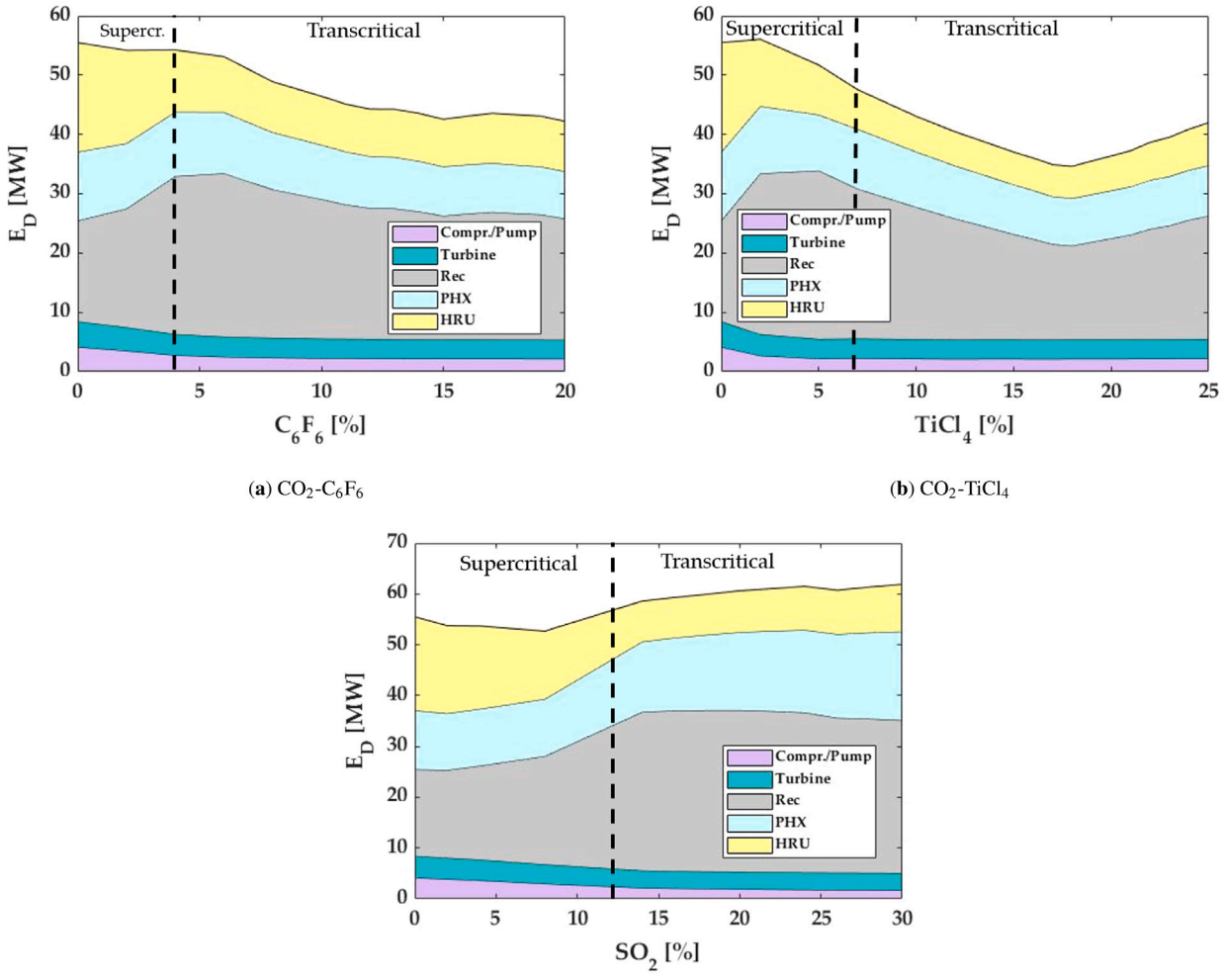

(**a**) CO_2-C_6F_6

(**b**) CO_2-$TiCl_4$

(**c**) CO_2-SO_2

Fig. 3. Breakdown of exergy destruction for *Recuperated Rankine* layout as function of dopant molar fraction. Different blends are considered.

starts increasing. This is due to the internal condensation of the mixture taking place inside the recuperator, which leads to an abrupt rise in hot stream specific heat capacity near the cold end of this heat exchanger. At the same time, and approximately in the same region of the recuperator, the cold stream heat capacity rises due to the proximity to the critical point. Fig. 4(b) provides a graphical representation of this circumstance for a 85%CO_2-15%C_6F_6 mixture. As a consequence, the internal condensation acts as a natural mechanism to balance the heat capacity of both streams, producing an increase in the exergy efficiency and a reduction of the exergy destruction. As a matter of fact, this effect is responsible of the good performance of CO_2-C_6F_6 and CO_2-$TiCl_4$ mixtures in the *Recuperated Rankine* layout, whilst exacerbates the increase in total exergy destruction in the CO_2-SO_2 case. Interestingly, this circumstance explains, from an exergetic standpoint, a conclusion obtained in previous works by the authors, i.e. the poor performance achieved by CO_2-SO_2 mixtures when combined with a simple recuperative cycle, and their great adaptability to a *Recompression* layout [35], as it will be discussed in the next paragraph of the present section. In fact, the narrow pressure–temperature envelope of these mixtures, as afore-commented in this manuscript, results to be the main driver for their poor and good performance with *Recuperated Rankine* and *Recompression* cycle, respectively, both effects brought by the lack of internal condensation in the recuperator.

Bearing all this in mind, the optimum cycle layouts for each mixture, identified in previous works by the authors, can be confirmed from a 2nd law standpoint. With this aim, *Precompression* layout is hereby taken into account for both CO_2-C_6F_6 and CO_2-$TiCl_4$ mixtures, whilst the *Recompression* is considered for CO_2-SO_2. Fig. 5 shows the breakdown of exergy destruction as a function of dopant molar fraction for these three cases. It can be observed that the optimum composition for CO_2-C_6F_6 and CO_2-$TiCl_4$ blends rounds 15% and 17% of dopant respectively, values extremely similar to the ones previously obtained in Fig. 3. Interestingly, a clear reduction of the exergy destroyed in the HTRec when passing from a supercritical to a transcritical embodiment can be observed in both cases (more information on this is provided later in this section). On the contrary, the optimum molar fraction of SO_2 employed in *Recompression* cycle results to be significantly different than the one obtained in Fig. 3(c) for a simple recuperative layout, and corresponds to a transcritical layout (see Fig. 5(b)). This circumstance is due to the fact that this cycle modification (i.e. split-compression) helps alleviating the large exergy destruction in the heat recuperator, which is the main drawback of increasing the molar fraction of SO_2, thus taking advantage of the vast reduction in the exergy destroyed in the HRU for molar content of SO_2 higher than 12%, brought by the condensing nature of the cycle. Even if the actual optimum corresponds to a 15% of SO_2, a higher molar fraction of dopant has been chosen in order to

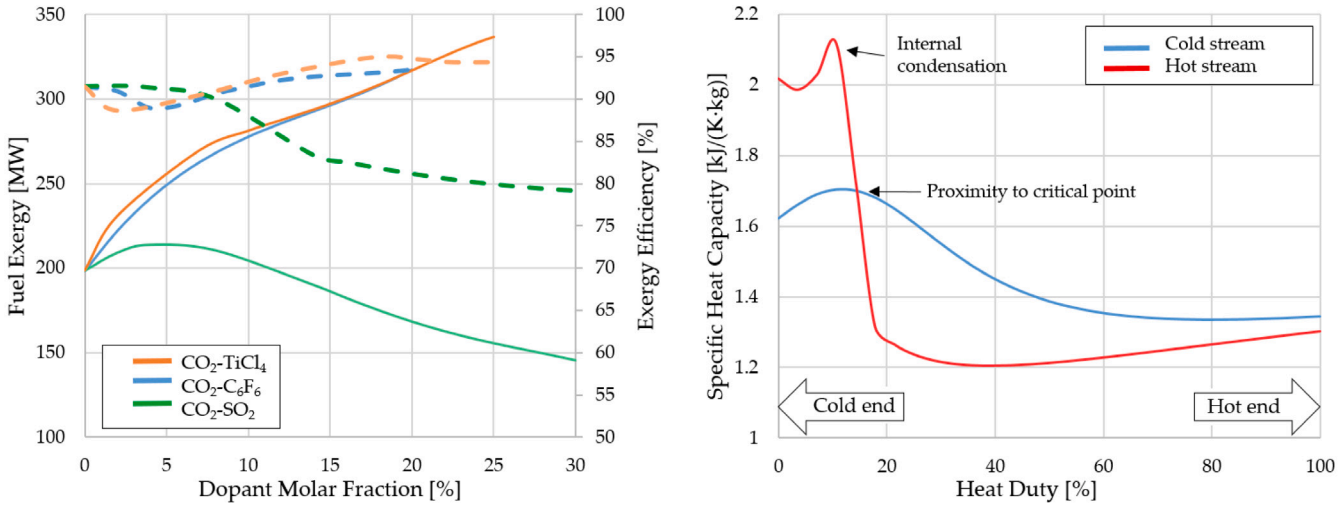

(**a**) Recuperator Fuel Exergy and Exergy efficiency

(**b**) Heat capacity inside the recuperator

Fig. 4. (a) Recuperator fuel exergy (solid lines) and exergy efficiency (dashed lines) as a function of the molar fraction for C_6F_6, $TiCl_4$ and SO_2, (b) Specific heat capacity [kJ/(kg K)] of cold and hot streams inside the recuperator, considering a 85%CO_2-15%C_6F_6 mixture.

guarantee a minimum temperature difference of roughly 15 °C between minimum cycle temperature and the resulting critical temperature of the blend [35]. This assumption, made for sake of security, ensures working fluid condensation even at minimum cycle temperatures up to 60 °C, corresponding to extreme ambient conditions.

Fig. 6 presents the exergy destruction breakdown for these three advanced layouts, as a function of the pressure ratio of the precompressor (PR_{PrC}) and the split-flow factor α, for *Precompression* and *Recompression* cycles respectively. This figure can be employed as a suitable tool to compare these advanced layouts against the simple recuperative configuration: if PR_{PrC} is equal to 1, in fact, the *Precompression* cycles converges to the *Recuperated Rankine* cycle; on the other hand, if α is set to 0, *Recompression* cycle is practically transformed into a *Recuperated Rankine* one. In this regards, several interesting observations can be made. Firstly, *Precompression* cycle is hereby confirmed to be able to improve the performance achieved by CO_2-C_6F_6 mixtures with respect to the *Recuperated Rankine* (PR_{PrC}=1), enabling a drop in the overall exergy destruction in the order of 14.6%, when PR_{PrC} is set to 1.41. On the contrary, the thermal performance enhancement obtained by using *Precompression* layout instead of *Recuperated Rankine* is very limited if CO_2-$TiCl_4$ mixtures are taken into account, with a maximum E_D reduction rounding 8%. This marginal gain in exergy efficiency, which corresponds as well to a slight increase in cycle thermal efficiency [24], does not seem to be sufficient to justify the use of the *Precompression* layout. For this reason, *Recuperated Rankine* is hence selected for CO_2-$TiCl_4$ blends, due to its expected better operability and lower capital cost, both features brought by its significantly simpler layout. Finally, for CO_2-SO_2 blends, the adoption of a *Recompression* cycle is clearly beneficial for cycle thermodynamic performance, as demonstrated by the impressive reduction in E_D >43%, obtained for α=38%. These circumstances confirm, from a exergy standpoint, the results obtained in previous works by the authors, which identified the following combination of best-performing cycle layouts and working fluid compositions: *Precompression* with 85%CO_2–15%C_6F_6, *Recuperated Rankine* with 83%CO_2–17%$TiCl_4$ and *Recompression* with 80%CO_2–20%SO_2.

It is worth noting that the improvement in cycle exergetic performance achieved by *Precompression* with CO_2-C_6F_6 and *Recompression* with CO_2-SO_2 is mainly caused, in both cases, by a significant reduction in the exergy destruction in heat recuperation process. Interestingly, these similar results are obtained by means of significantly different thermodynamic behaviours of these two cycle configurations. The *Precompression* cycle provokes a twofold effect: on the one hand, it increases the specific work, overcoming the constraint imposed on turbine exhaust pressure by the pump inlet one, which is fixed, for a given minimum cycle temperature, due to the condensing nature of the cycle; on the other hand, the turbine outlet temperature diminishes, with a consequent reduction in heat recuperation potential of this cycle. The reduction of the circulating mass flow affects, from an exergy perspective, all exergy flows equally, but only translates into an overall reduction of the exergy destruction in the pump and the HRU. In the turbine, the higher expansion ratio of the cycle leads to a grow in the specific exergy destruction (kJ/kg) which completely counterbalances the reduction in the mass flow, leading to a larger exergy destruction as net effect. Similarly, the lower turbine outlet temperature results in a higher temperature rise in the PHX, increasing its exergy destruction. Obviously, the inclusion of the precompressor adds a new source of irreversibility, associated to the compression of the fluid in gas phase. In the recuperators, opposing trends for the exergy destruction can be observed for the LTRec and HTRec, an increasing one in the former and a decreasing one in the latter. This is due to a redistribution of the heat recovered in these two components, which is progressively shifted towards the LTRec, as can be seen by looking at the trends of fuel exergy in Fig. 7(a), represented in solid line. The overall reduction of the exergy destruction in the heat recuperation (sum of the contribution of LTRec and HTRec) cannot be only attributed to the reduction of the mass flow, but to an enhancement of the exergy efficiency in the recuperation. In Fig. 7(a), the impact of the PR_{PrC} on the exergy efficiency of LTRec and HTRec is depicted with dashed lines. It can be seen that both exergy efficiencies grow with PR_{PrC}, concluding that the addition of a compressor in the low-pressure side of the cycle, besides enhancing specific work, also contributes to a reduction of the irreversibility in the heat recuperation. On the contrary, the split-flow stratagem employed in the *Recompression* happens to penalise specific work. From an exergy perspective, the larger mass flow provokes the growth in the exergy destruction in the turbomachinery (pump, turbine and recompressor). On the other hand, the reduction in the exergy destruction experimented by the PHX and, more importantly, by the HRU, leads to a higher internal heat recuperation, which reduces the heat duty in both equipment. Nevertheless, the larger amount of recuperated heat does not translate into a rise in the exergy destroyed in the recuperators (sum of LTRec and HTRec) but, conversely, to its

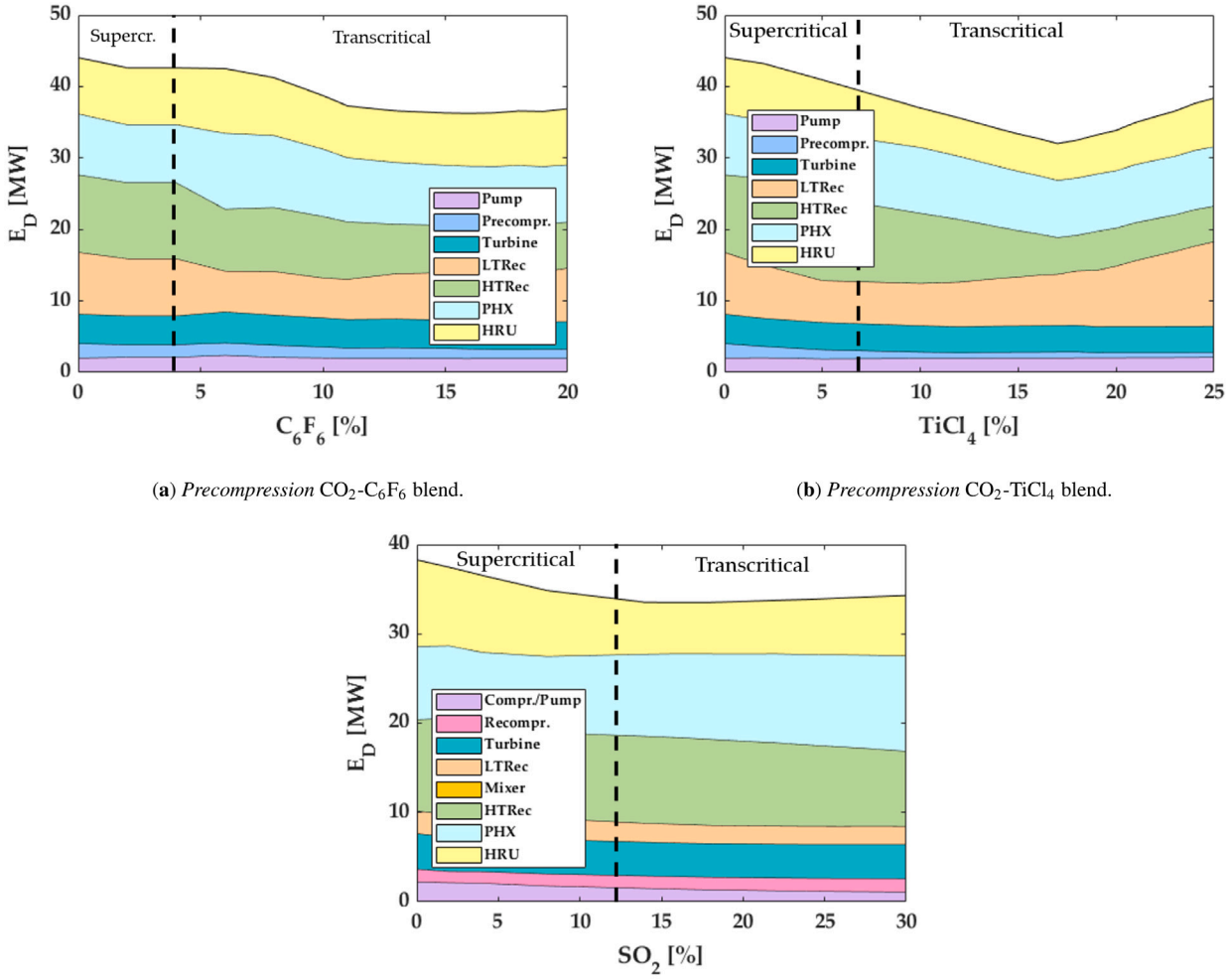

(**a**) *Precompression* CO_2-C_6F_6 blend.

(**b**) *Precompression* CO_2-$TiCl_4$ blend.

(**c**) *Recompression* with CO_2-SO_2 blend.

Fig. 5. Breakdown of exergy destruction for *Precompression* (a, b) and *Recompression* (c) layouts, as function of dopant molar fraction. Different blends are considered.

important reduction. Fig. 7(b) explains this circumstance: on the one hand, the fuel exergy remains almost constant in the HTRec (red solid line) and increases in the LTRec (blue solid line), meaning that the majority of the available heat is being recuperated in the cold side of the cycle. On the other hand, the exergy efficiency of both the LTRec and the HTRec increases with the split-flow factor, being this the main driver of the overall reduction in the exergy destroyed during heat recuperation process. Finally, it is worth noting that another (slight) source of irreversibility appears, brought by the non-isothermal mixing of the streams. In this regard, it can be observed that the destruction of exergy in the mixer is reduced to zero when considering the optimal split-flow factor, due to the fact that, under these conditions, the mixing process takes place at a constant temperature [12].

Once the best-performing cycle layouts are identified for each blend, these are duly optimised in order to maximise their thermal efficiency employing MATLAB's 'Global Optimisation Toolbox', together with the pure-CO_2 configurations considered in this study. The complete set of optimum cycle specifications is now provided in Table 6, for both energy source temperatures taken into account. The parameters to be optimised, previously presented in Section 2, are: main compressor/main pump pressure ratio (PR_{MC}), precompressor pressure patio (PR_{PrC}) and split-flow fraction (α). The value of the resulting turbine expansion ratio (ER_T) is also indicated in the table, although it is linked to the previous parameters, hence it cannot be properly considered as a free optimisable parameter. Moreover, for sake of completeness, the heat and mass balances of all cycle configurations can be found in Appendix.

4.2. Exergy analysis and comparison of steam turbines and CO_2-based power cycles

The main results obtained from the 1st and 2nd Law analyses are summarised in Table 7 for the two energy source temperatures levels considered. Cycle thermal efficiency (η_{th}), exergy efficiency (ϵ_{cyc}) and exergy destruction (E_D) are taken into account as main figures of merit. On the other hand, temperature rise across the primary heat exchanger (ΔT_{PHX}) and specific work W_s are considered as well in the comparison. A volumetric specific work, expressed in MJ/m^3 and referred to the volumetric flow rate measured at turbine inlet, is preferred against the traditional specific work in kJ/kg in order to account for the actual footprint of the components, affected by the different density of the various working fluid hereby studied. Furthermore, it is to note that ΔT_{PHX} is of extreme importance inasmuch as it affects the temperature rise across the solar receiver and, therefore, the final size and cost of the entire solar subsystem (most notably the receiver and Thermal Energy Storage system). In particular, this size can be reduced with higher values of ΔT_{PHX} and this effect has been proven as important as the

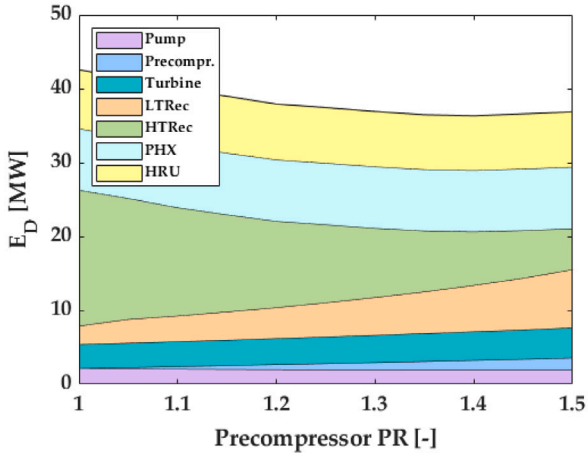

(**a**) *Precompression* with 85%CO_2-15%C_6F_6 blend

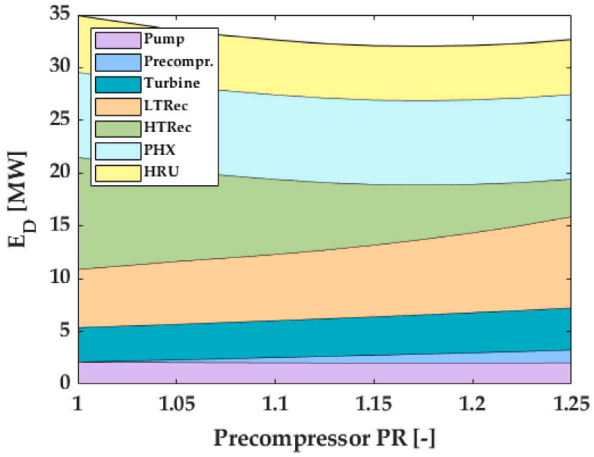

(**b**) *Precompression* with 83%CO_2-17%$TiCl_4$ blend

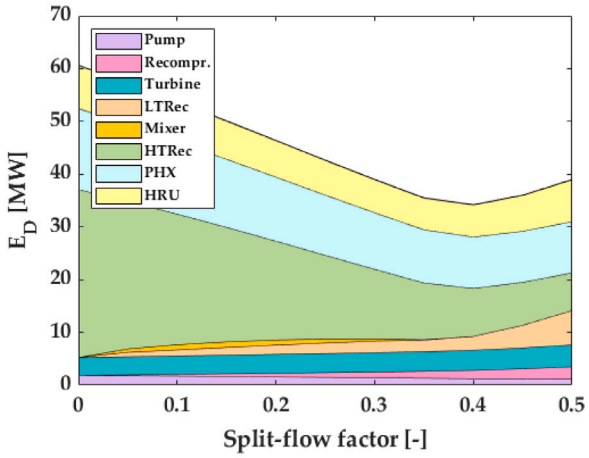

(**c**) *Recompression* with 80%CO_2-20%SO_2 blend

Fig. 6. Breakdown of exergy destruction for *Precompression* (a, b) and *Recompression* (c) layouts, as function of PR_{Prc} and α respectively. Different blends are considered.

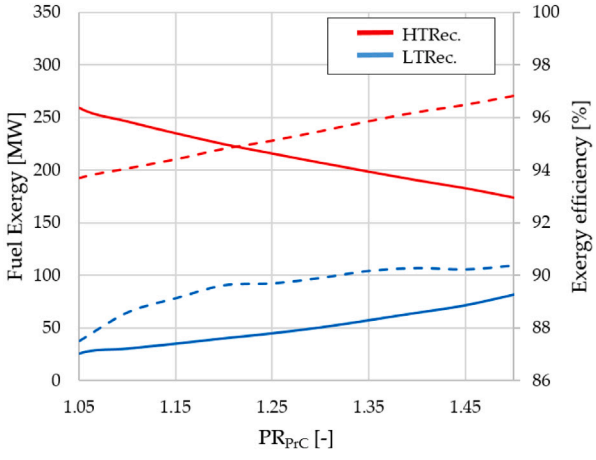

(**a**) *Precompression* with 85%CO_2-15%C_6F_6 blend

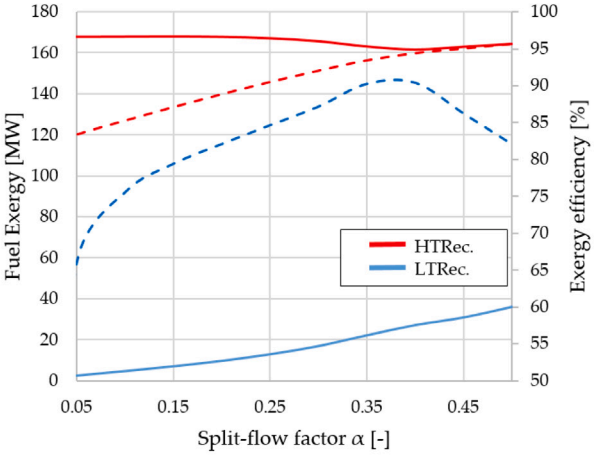

(**b**) *Recompression* with 80%CO_2-20%SO_2 blend

Fig. 7. Fuel exergy (solid lines) and exergy efficiency (dashes lines) of Low-temperature and High-temperature recuperators as a function of Precompressor Pressure Ratio (PR_{PrC}) and split-flow factor (α). Different cycles and blends are considered.

Table 7
Results for the five different cycles and two energy source temperatures (575/725 °C).

Cycle	η_{th} [%]	ϵ_{cyc} [%]	ΔT_{PHX} [°C]	W_s [MJ/m^3]	E_D [MW]
SoA Rankine	43.9/45.6	69.7/66.6	309.1/352.1	54.4/65.78	43.3/50.0
RC sCO_2	42.9/49.7	68.0/72.4	132.9/150.5	10.5/11.6	47.1/38.2
PC sCO_2	42.1/49.1	66.7/71.6	189.1/225.1	14.6/17.2	50.0/39.7
PrC D1	43.6/50.4	69.2/73.4	148.6/166.1	18.8/20.5	44.6/36.2
RR D2	45.7/51.6	72.4/75.3	138.3/158.7	15.0/15.7	38.1/32.9
RC D3	44.8/51.3	71.1/74.8	177.2/200.7	15.0/16.2	40.7/33.7

impact of η_{th} to influence the overall thermo-economics of the plant [6]. As a consequence, even if the present paper does not openly develop the thermo-economic features of the cycles considered, these parameters are still kept in the analysis as an indirect metric to account for these aspects of plant performance.

At 575 °C (corresponding to TIT=550 °C), Rankine cycles working on steam outperform pure sCO_2 cycles for all figures of merit: >1–2 pp higher thermal and exergy efficiency, lower E_D (4–7 MW) and a >120 °C higher ΔT_{PHX}. For sCO_2 mixtures, the PrC D1 exhibits performances comparable to the ones obtained by SoA Rankine, while the RC D3 and, especially, the RR D2 exceed that of steam Rankine in terms of thermal and exergy efficiency by >0.9–1.8 and >1.4–2.7 pp, respectively. Unalike values for the ΔT_{PHX} are obtained: low for the PrC D1 and RR D2 and higher for the RC D3, but in all cases below that of the SoA Rankine. All this implies that a thermodynamic gain is to be expected from the SCARABEUS technology even at 550 °C but how much this translates into a true techno-economic benefit is yet to be determined; further economic analysis is needed, in particular for the solar subsystem.

Considering the higher energy source temperature (725 °C), the behaviour of the steam Rankine cycle changes significantly. Live steam temperature is set to a maximum of 600 °C, widely considered as a threshold temperature for cost-effective steam-based Rankine cycle. This brings about a large turbine inlet temperature gap between the steam and sCO_2 cases which leads to a significant reduction in exergy efficiency of the steam Rankine case due to the much larger exergy destruction during heat addition. For these reasons, the previous case at 575 °C is identified as the best-candidate for steam-based cycles and used as reference for the comparison with CO_2-based technology, independently on the temperature level considered. On the contrary, pure sCO_2 power cycles exploit the higher TIT successfully, achieving a significant improvement in cycle exergy efficiency, in the order of 4–5 pp. This translates into thermal and exergy efficiencies around 49% and 72%, with gains with respect to SoA Rankine up to 5.8 pp and 2.7 pp, respectively. The improvement in 'thermodynamic quality' of the CO_2 mixtures cycles is also noteworthy: +5 pp for PrC D1, +4.4 pp for RR D2 and +3.7 pp for RC D3 in exergy efficiency. The thermal efficiency of the three configuration exceeds 50% (>6.5–7.7 pp than SoA Rankine), whereas the exergy efficiency ranges from 73.4% to 75.3% (>3.7–5.6 pp than SoA Rankine). Among the five CO_2-based technologies considered, those based on CO_2 mixtures clearly outperform pure sCO_2 ones in thermodynamic terms: >1–2 pp higher η_{th}, 1–3 pp higher ϵ_{cyc} and 6%–14% lower E_D. On the other hand, the analysis of the secondary figures of merit provide multiple insights: (i) although PC CO_2 is slightly worse than RC CO_2 in thermal (<0.6 pp) and exergy (<0.8 pp) efficiencies, the improvement in ΔT_{PHX} (>50%) and W_s (>48%) tilts the scale in favour of the former; (ii) in the same way for the CO_2 mixtures, the slightly worse thermodynamic performance of RC D3 against RR D2 (<0.2 pp thermal efficiency, <0.5 pp exergy efficiency) is greatly counterbalanced by a higher ΔT_{PHX} (>26%), with similar W_s (>3%). As a drawback, CO_2 mixtures significantly reduce the ΔT_{PHX} with respect to SoA Rankine (<35%) which, along with the need for advanced molten salts that can withstand 725 °C, raises important concerns about the cost of the Thermal Energy Storage for these systems. Nevertheless, it is worth noting that this circumstance is also an issue for pure sCO_2 technology at high temperature, and even more critical in the RC CO_2 due to its very low ΔT_{PHX} (<25% than RC D3).

The rightmost column in Table 7 shows that, for a given exergy product (set to 100 MW), the largest destruction of exergy is found for pure sCO_2 and steam Rankine for energy source temperatures of 575 °C and 725 °C respectively. On the contrary, sCO_2 mixtures always present the lowest E_D, hence ensuring an enhanced exergy performance as compared to pure sCO_2 and even steam. In order to assess where this improvement comes from, a closer look into the constituents of E_D for each cycle is presented below. To this end, cycle components have been organised in five categories: turbine, primary heat exchanger (PHX), recuperators, compression devices and heat rejection unit (HRU) [33]. The breakdown of the exergy destroyed in each cycle configurations, divided by category, are shown in Figs. 8 and 9, in absolute and percentage terms respectively. Furthermore, the complete heat & mass balances and a resume of exergy balances by components of the different CO_2-based systems can be found in Appendix, for both heat source temperatures. This information confirms the conclusions in past works such as Angelino's [13]: in steam Rankine cycles, exergy destruction takes place mostly in the primary heat exchanger PHX (around 65%) whereas losses spread somewhat evenly across several components in pure sCO_2 cycles. If sCO_2 mixtures are used, then the pattern sits in between the other two cases: the contribution to the total exergy destruction of the compression devices and the HRU are reduced for the three blends. Nevertheless, this improvement comes at the cost of a (slightly) higher share of the exergy destruction in the recuperators for PrC D1 and RR D2 and the exergy destruction in the PHX for RC D3.

This change of the exergy destruction pattern is enabled by the modified properties of the working fluid when additives are added to Carbon Dioxide and suggest that the SCARABEUS concept is a sound approach to inherently more efficient Concentrated Solar Power plants. This is confirmed by the very similar trends observed for the two energy source temperatures studied, which is an indicator of the general applicability of the behaviour observed. At the same time though, the amount of exergy destroyed across the recuperator of blended sCO_2 cycles also reveals the need for further cycle optimisation, probably figuring out new layouts where this irreversibility can be reduced without increasing exergy destruction at another component. This has already been tackled for pure sCO_2; for instance, the development of the *Recompression* and *Partial Cooling* cycles by Angelino (1968) [12] aimed to reduce the irreversibility brought about by the recuperators in order to enhance cycle performance.

The potential of a power cycle to improve to a greater or lesser extent its exergy efficiency when moving to higher TIT is influenced by its degrees of freedom for cycle optimisation. In this regard, those cycles incorporating a Precompressor in their layouts shows a higher relative exergy destruction reduction when increasing TIT from 550 °C to 700 °C. In particular, the PC CO_2 experiences an E_D decrease of 10.4 MW against the 8.9 MW for RC CO_2, whereas the PrC D1 exhibits a reduction in 8.4 MW against the 5.1 MW of RR D2 and 7 MW of RC D3. This statement is supported by looking at how the optimum specification changes between the 575 °C and 725 °C cases in Table 6: the split-flow factor for RC CO_2, PC CO_2 and RC D3 as well as the optimum molar fraction for the three CO_2 mixture are almost constant for both temperature levels. On the contrary, the optimum PR_{PrC} increases significantly at higher TIT, aiming at achieving a rise in the turbine expansion ratio (ER_T).

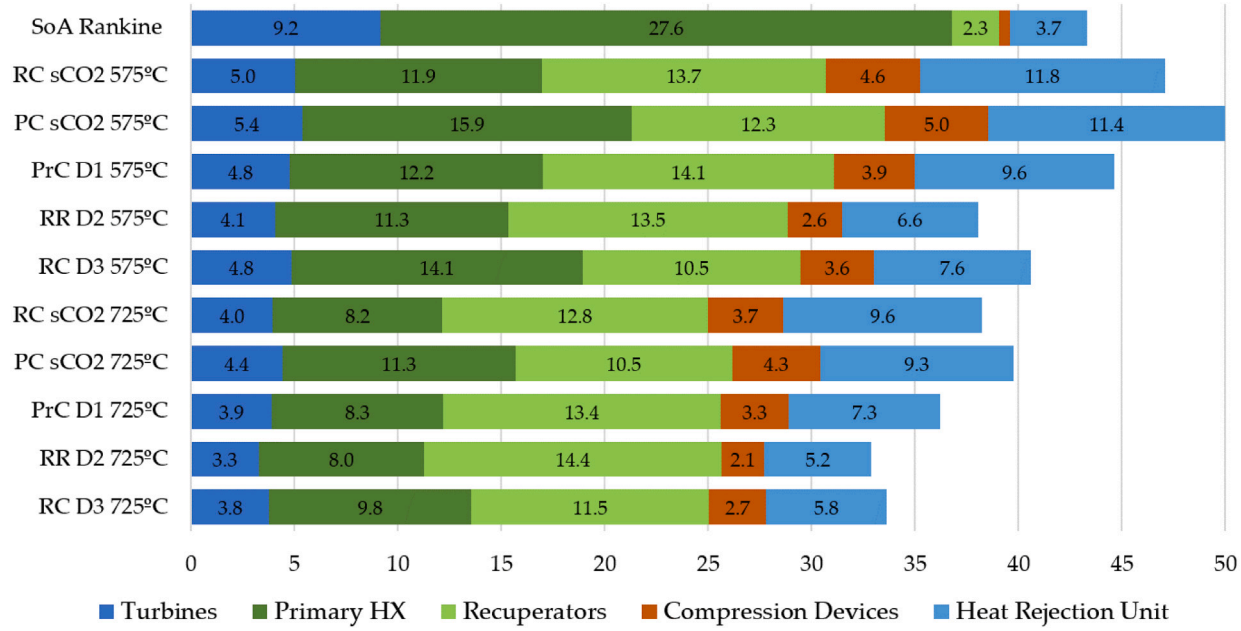

Fig. 8. Breakdown of exergy destruction for different combinations of cycles, fluid and Turbine Inlet Temperatures (TIT). Labels and axis refer to E_D expressed in absolute terms (MW).

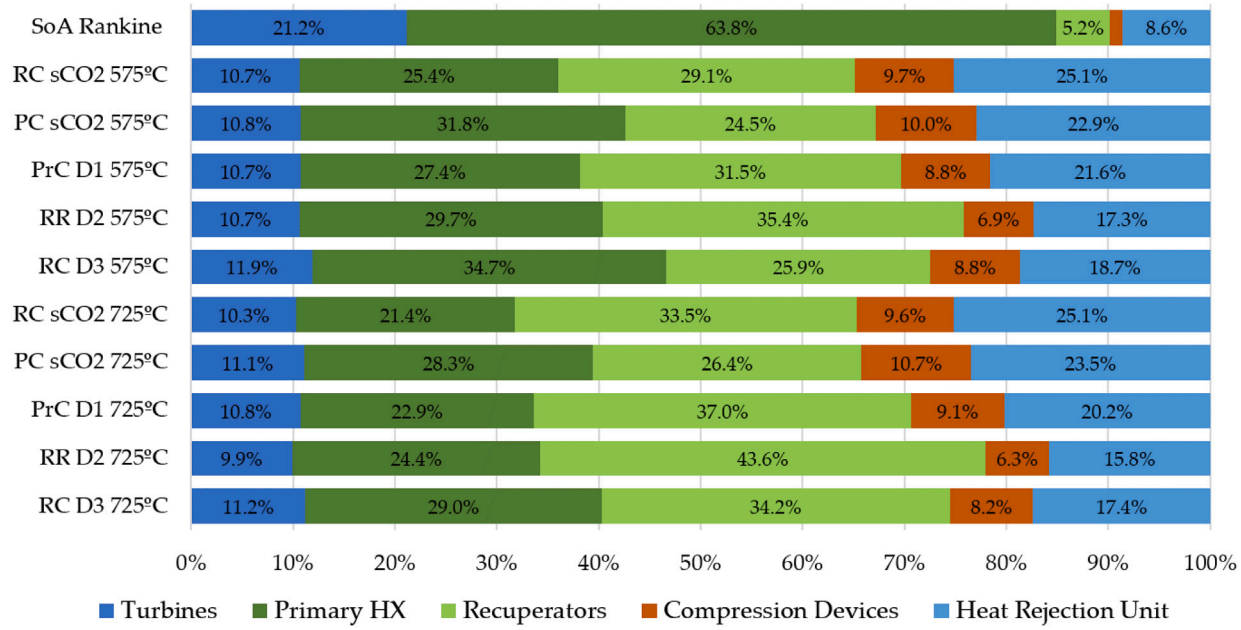

Fig. 9. Breakdown of exergy destruction for different combinations of cycles, fluid and Turbine Inlet Temperatures (TIT). Labels and axis refer to E_D expressed in percentage terms (%).

Fig. 10 compares the *Efficiency losses from Carnot Cycle* for the five different cycle configurations considered, using a similar colour code to Figs. 8 and 9. This is a very useful information to identify the root causes for the thermal efficiency drop with respect to the reference Carnot cycle since η_{th} can be obtained by merely subtracting the total losses indicated in Fig. 10 (also second column in Table 7) from the efficiency of a Carnot cycle working between the same heat source (725 °C) and heat sink (40 °C) temperatures: 68.6%. Moreover, $\Delta\eta_k$ also allows to "normalise" the results obtained previously with a common reference for energy input, hence overcoming the difference in overall fuel exergy introduced to the cycle (unavoidable, as it is brought about by the different values of ΔT_{PHX}). The results provided are in agreement with those shown earlier in this section, confirming that condensation of the working fluid leads to a considerable reduction in the thermodynamic losses (with respect to Carnot efficiency) across the compression and heat rejection processes. All sCO_2-based configurations concentrate roughly the same overall irreversibility in turbine, PHX and recuperators (13%). Conversely, an important difference in the cumulative value of $\Delta\eta_k$ across the compression devices and HRU is found: 6%–7% for pure sCO_2 and 3%–5% for blended sCO_2. It is

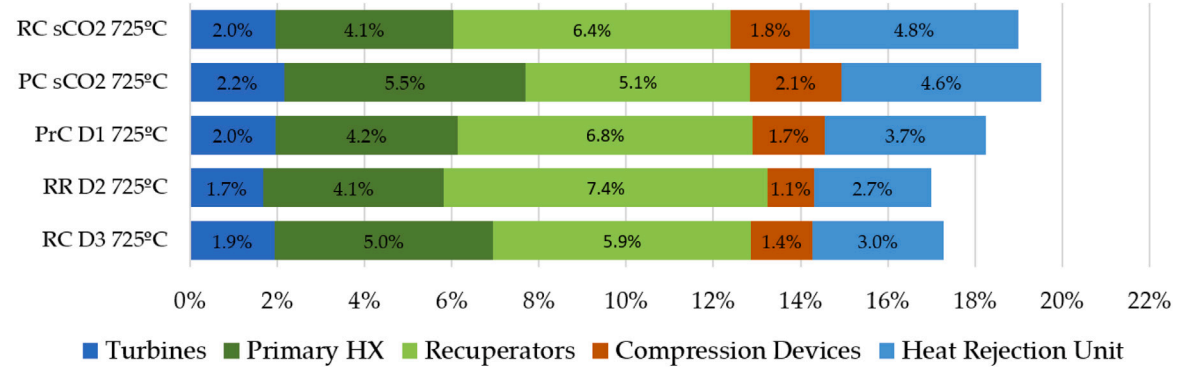

Fig. 10. *Efficiency losses from Carnot Cycle* for five different sCO_2-based cycles, considering a heat source temperature of 725 °C.

therefore thanks to this difference that using sCO_2 mixtures enables better 2nd Law performance of both the *Recompression* and *Partial Cooling* cycles working with pure sCO_2.

4.3. Sensitivity of exergy efficiency to maximum cycle pressure

Maximum pressure results to be a key-parameter for power cycle thermo-economic optimisation. This is perfectly demonstrated in the seminal works by Gianfranco Angelino, in which a sensitivity analysis obtained varying this parameter and considering the *Efficiency losses from Carnot Cycle* as main figure of merit is performed for pure sCO_2 cycles, both under transcritical [12] and supercritical [13] embodiment. From an exergetic standpoint, Angelino observed that the increase in the maximum cycle pressure produces the following effects: (1) a rise in the exergy destruction in the PHX, brought by the lower turbine outlet temperature; (2) an increase in the exergy destroyed in the HRU, caused by the higher pump outlet temperature; (3) a higher exergy destruction in the turbine and the main compressor (pump in transcritical cycles), brought by the larger pressure ratio; (4) a reduction in the exergy destruction in the recuperators due to the lower heat recuperated, partly because of the lower turbine outlet temperature but also thanks to the enhancement in the specific work. Moreover, the exergy efficiency of the heat recuperation is prone to increasing because the cold stream (pump outlet) and the hot stream (turbine outlet) temperatures are closer. Therefore, the optimum P_{max}, in terms of minimum exergy destruction (i.e maximum cycle exergy efficiency), is the trade-off between the rise in exergy destruction in the PHX, HRU and turbomachinery and the drop in the exergy destroyed in the recuperators. In this regard, sCO_2 power cycles are characterised by an extremely high optimum maximum cycle pressure, which can be well beyond 400 bar for some cycle configurations [46,47]. Nevertheless, such pressure levels are the results of purely thermodynamic analysis and, even if they can provide useful information regarding the inner thermodynamic behaviour of the different cycle configurations, they are not feasible from a practical standpoint [6]. In literature, it is a common practice to consider a lower level of P_{max}, usually rounding 250–300 bar [5,33], being this a threshold value representing a reasonable techno-economic optimum for sCO_2 technology. Nevertheless, it is not clear whether or not the assumed value of 250 bar is far from the real optimum for the innovative power systems investigated by SCARABEUS consortium. In order to provide a preliminary answer to this question, the influence of the maximum cycle pressure (P_{max}) on cycle exergy efficiency and optimum molar fraction is investigated by means of a sensitivity analysis, considering the three best-performing SCARABEUS systems previously identified in this paper. To this aim, P_{max} is varied from 200 up to 350 bar, considering the same ranges of dopant molar fraction employed in Section 4.1, for transcritical embodiment only.

Fig. 11 shows the trend of cycle exergy efficiency as a function of dopant molar fraction and maximum pressure by means of a combined surf+contour maps, obtained optimising the three cycles considering each different possible combination of these two parameters. Interestingly, it can be noticed that the three blends present significantly different exergy efficiency overall patterns. The *Precompression* operated with C_6F_6 presents an exergy efficiency rounding 71%–74% for any possible combination of boundary conditions, being barely affected by the variation in P_{max}, and only slightly by the dopant molar fraction. As a matter of fact, ϵ_{cyc} happens to be constant for C_6F_6 molar content higher than 10%, creating a plateau-like pattern. On the contrary, the exergy performance of the *Recuperated Rankine* with $TiCl_4$ seems to be really sensitive to variations in both P_{max} and dopant molar fraction, with values ranging 65%–75%. Finally, the ϵ_{cyc} achieved by *Recompression* with SO_2 is barely affected by changes in dopant molar content, but presents a slightly increasing trend with P_{max}, passing from 73% up to 76% at 200 and 350 bar respectively. Focusing on the optimum composition for each different system, it is worth noting that this barely depends on P_{max}, showing just a small tendency towards lower molar fraction in the RR D2 case at pressures higher than 300 bar. This confirms the results obtained in [34], i.e. that, for a given cycle layout, the optimum blend composition is mainly a function of minimum cycle temperature (see Section 4.4), and it is affected only slightly by turbine inlet temperature or P_{max}.

In order to provide a comprehensive explanation to this heterogeneous scenario, an analysis on how the exergy destruction is distributed amongst the different equipment as a function of P_{max} results to be mandatory. In this regard, Fig. 12 depicts E_D stacked area plots, similar to the ones already presented in Fig. 3, for the optimum molar fraction previously identified for a maximum pressure of 250 bar (see Section 4.1), thus following the black dashed lines provided in Fig. 11. Considering PrC D1 (Fig. 12(a)), the rise in P_{max} leads to a gradual redistribution of the exergy destruction among the various components, resulting in a constant value of E_D and, at a larger extent, ϵ_{cyc}. The slight decrease in the E_D of the LTRec and HTRec, in fact, is not capable of counterbalancing the rise in the exergy destruction in all other components. This can be better understood observing Fig. 13, which depicts the variation of the exergy efficiency of the recuperators with P_{max}. For the PrC D1 case (blue lines in Fig. 13), the impact on both LTRec and HTRec is minimum, with deviations in the order of 1 percentage point for both equipment. Actually, it is also observed that the exergy destruction in the Precompressor experienced a significant decrease, indicating that the optimum PR_{Prc} is reduced with P_{max}.

On the other hand, the RC D3 system shows a somewhat more conventional pattern, similar to that of a pure-CO_2 condensing cycle (see Figure 13(c) from [12]): a large reduction in the exergy destruction of the recuperators, partially counter-balanced by the higher E_D in

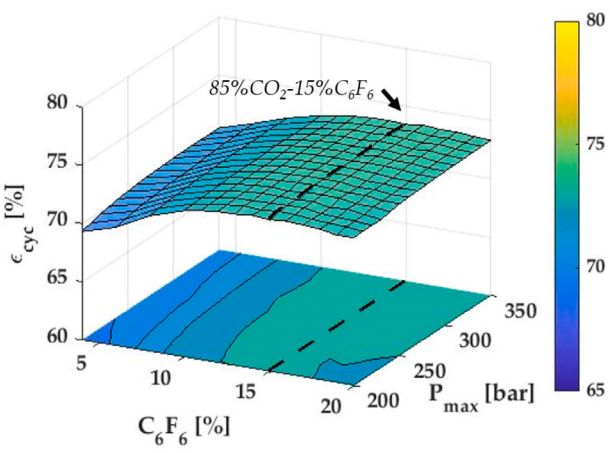

(**a**) *Precompression* with CO_2-C_6F_6 mixtures.

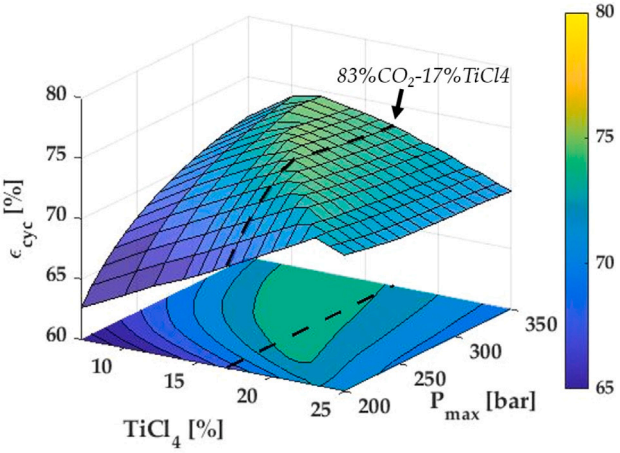

(**b**) *Recuperated Rankine* with CO_2-$TiCl_4$ mixtures.

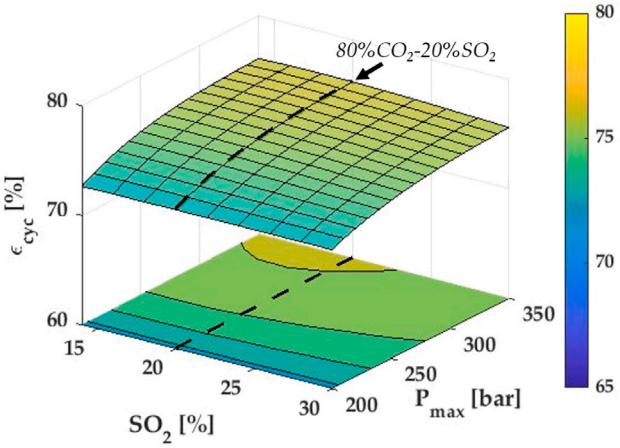

(**c**) *Recompression* with CO_2-SO_2 mixtures.

Fig. 11. Influence of P_{max} and dopant molar fraction on cycle exergy efficiency. A turbine inlet temperature of 700 °C is considered, employing different cycle layouts and mixtures.

the PHX and, to a lesser extend, the turbomachinery and the HRU. Fig. 13 for RC D3 reveals an improvement of the exergy efficiency of both recuperators, especially important in the LTRec (+4 pp). On the contrary, the RR D2 system presents a very interesting pattern, significantly different from what could be expected for a *Recuperated Rankine* cycle (see Figure 13(b) from [12]) and directly influenced by the wide PT envelope that characterises CO_2-$TiCl_4$ mixtures. Considering low P_{max} values, the pump outlet results to be lower than the cricondenbar pressure (around 240 bar for 17% $TiCl_4$, see Fig. 2(b)). This means that, even if the maximum pressure is higher than the critical one, the working fluid passes through the saturation dome while being heated up in the recuperator. The subsequent rise in the high-pressure streams heat capacity penalises the exergy efficiency of this equipment, explaining its large exergy destruction. Secondly, when P_{max} exceeds the cricondenbar pressure, it soon gets to an optimum (around 260 bar), after which the total exergy destruction starts rising again. Observing the stacked areas, it is clear that the decrease in the E_D in the recuperator is not sufficient to compensate the increase in the PHX, turbomachinery and HRU at high P_{max}. The reason for that is that the higher pressure ratio of the cycle implies a higher temperature rise in the pump, which in turn pushes the HRU inlet out of the saturation dome. In other words, increasing maximum cycle pressure beyond the cricondenbar penalises the internal condensation in the Recuperator which, as previously commented in Section 4.1, is the main driver of the extremely good thermal performance of this system. This behaviour is observed in Fig. 13 for the RR D2 case: the exergy efficiency of the recuperator increases 1 pp as P_{max} approximates the cricondenbar, then reaches a maximum coinciding with the P_{max} of maximum cycle exergy efficiency and, from that point and on, decreases uninterruptedly due to the lesser internal condensation.

As a final conclusion, this section reveals that, for the SCARABEUS systems in analysis, there is just a limited interest in considering maximum pressures significantly higher than 250 bar, and this threshold value could be even reduced to 200 bar if a *Precompression* with C_6F_6 is considered. This result is extremely promising from a techno-economic standpoint, since it confirms the potential SCARABEUS concept to achieve outstanding thermal performances without requiring very high pressures, which significantly increases capital costs and complicates the design of various cycle components.

4.4. Sensitivity of exergy efficiency to minimum cycle temperature

The results discussed in previous sections have been obtained considering a minimum cycle temperature of 50 °C. This value has been set referring to typical ambient conditions of CSP plants, usually located in sites with high Direct Normal Irradiation (DNI) and high ambient temperatures (often rounding 35–40 °C [48]). Nevertheless, the

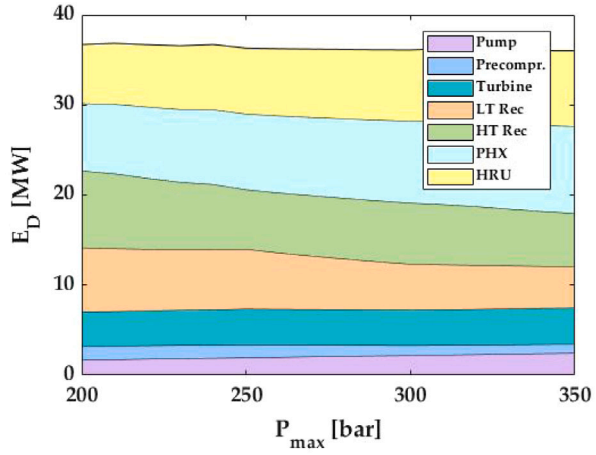

(**a**) *Precompression* 85%CO_2-15%C_6F_6 700ºC

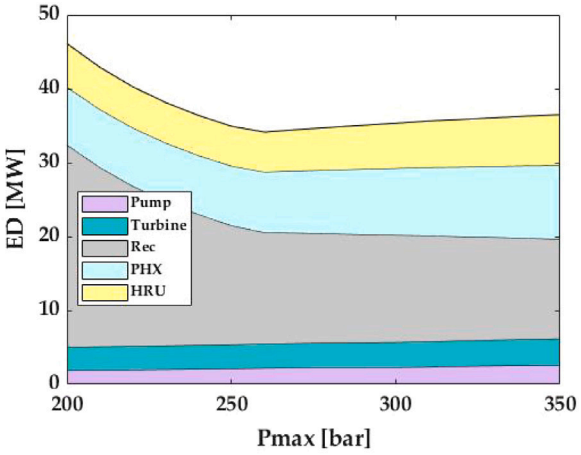

(**b**) *Recuperated Rankine* 83%CO_2-17%$TiCl_4$ 700ºC

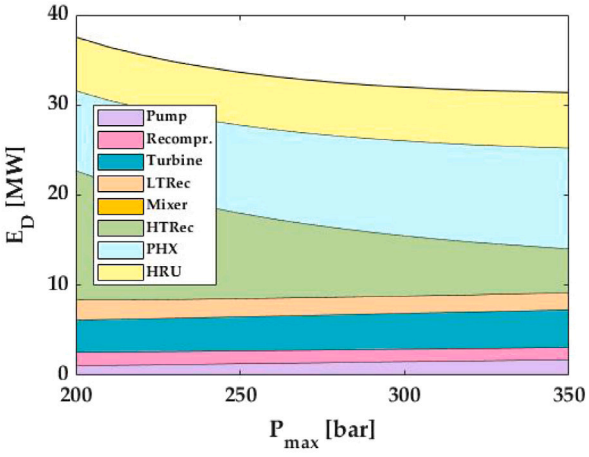

(**c**) *Recompression* 80%CO_2 − 20%CO_2 700ºC

Fig. 12. Breakdown of exergy destruction as function of maximum cycle pressure. Different combinations of blend and cycle layout are considered.

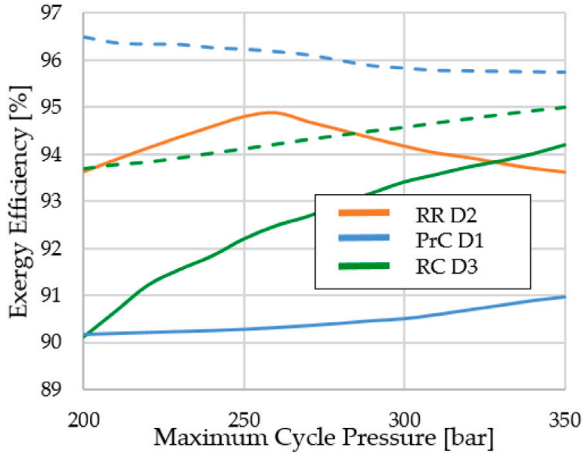

Fig. 13. Recuperator exergy efficiency as a function of maximum cycle pressure. Different combinations of blend and cycle layout are considered. Solid lines for LTRec and dashed lines for HTRec, when applicable.

SCARABEUS concept, similarly to pure sCO_2 technology, is prone to be extrapolated to other application fields, characterised by a wide range of ambient temperatures. Therefore, a sensitivity analysis varying minimum cycle temperature is undertaken, in order to analyse the capability of SCARABEUS systems to maintain their good thermal performance with difference ambient conditions, comparing it against pure sCO_2 technology. To this aim, minimum cycle temperatures from 35 °C to 60 °C are hereby taken into account, and the exergy efficiencies of the different systems are then calculated considering a 10 °C lower cold source temperature (25 °C–50 °C). A hot source temperature of 725 °C is taken into account, and the remaining boundary conditions are the ones previously indicated in Table 1. For each minimum cycle temperature, the entire set of CO_2-based systems have been duly optimised, following the same rationale discussed in Section 4.1. The results of this sensitivity analysis are provided in Fig. 14 as a function of minimum cycle temperature, showing that the three SCARABEUS systems present a significantly less steep trend with respect to pure CO_2 ones. In particular, *Precompression* cycle with D1, *Recuperated Rankine* cycle with D2 and *Recompression* cycle with D3 show an exergy efficiency reduction rounding 2.4, 3.5, 3.2 percentage points respectively, against the 5.2 and 4.1 pp drop observed in *Recompression* and *Partial Cooling* operated with pure CO_2. These results utterly confirm the stronger adaptability to high ambient temperatures that characterises SCARABEUS systems, which enable exergy efficiency gains up to 3 percentage points with

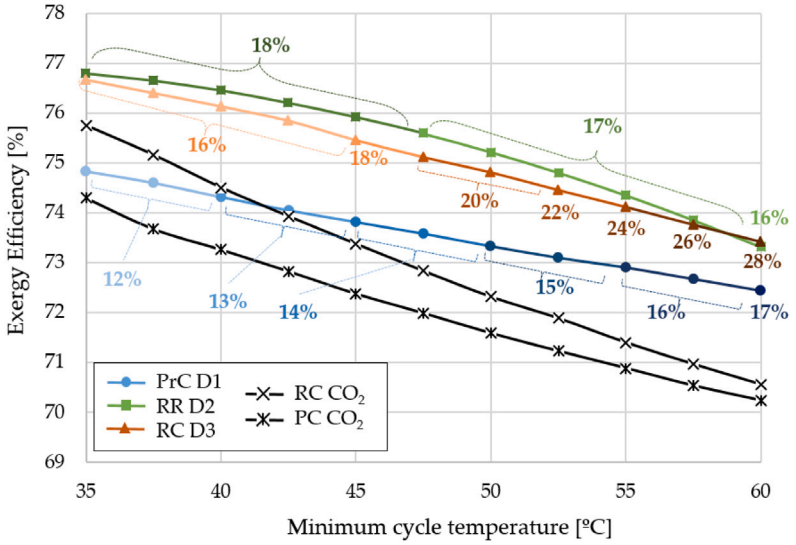

Fig. 14. Cycle exergy efficiency as a function of minimum cycle temperature. Five different combinations of working fluid and cycle layout are considered.

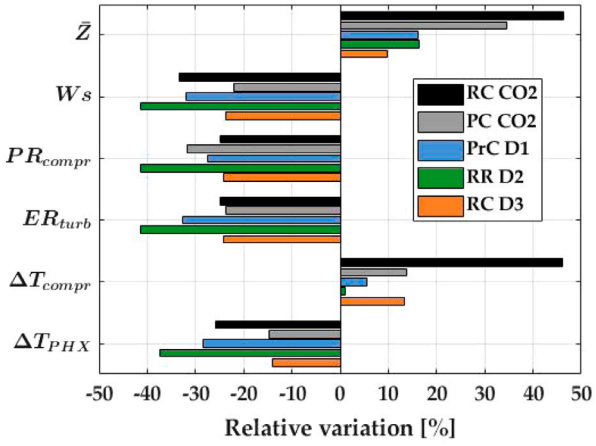

Fig. 15. Relative difference in main cycle indicators when minimum cycle temperature increases from 35 °C to 60 °C. Five different combinations of working fluid and cycle layout are considered.

respect to the pure CO_2 cycles if a minimum cycle temperature of 60 °C is considered. On the contrary, the interest in CO_2-blend seems not to be justified at low temperature levels, where the performance of pure CO_2 systems are extremely enhanced (compression process can be operated in the extreme vicinity of the critical point). As a matter of fact, the exergy efficiency gains achieved by SCARABEUS systems is reduced to (roughly) 1 percentage point at 35 °C, and in some cases the pure CO_2 performs even better than the blended solution (see RC CO_2 and PrC D1, Fig. 14).

The trends shown in Fig. 14 can be explained by reasoning about the optimisation rationale specific to each system, observing how the corresponding optimisable parameters are adapted when the minimum temperature of the design cycle is increased. In this regard, Fig. 15 depicts the relative variation of some relevant cycle parameters, namely mean compressibility factor $\bar{Z}$ (i.e., arithmetic average between main compressor inlet and outlet conditions), specific work (W_s), main compressor/pump pressure ratio (PR_{compr}), turbine expansion ratio (ER_{turb}), temperature rise in the compression process (ΔT_{compr}) and temperature rise across Primary Heat Exchanger (ΔT_{PHX}). This last parameter results to be particularly, since it is an indicator of the heat recuperation potential of a cycle (the greater the amount of heat internally recovered, the lower the ΔT_{PHX}), as well as the size and cost of the TES (the lower the ΔT_{PHX}, the bigger the TES).

As already commented in Section 2, two main differences can be identified between pure and blended CO_2-based systems: on the one hand, the pressure at the inlet of the main compressor/pump (cycle station 1 in Fig. 1) can be optimised independently in pure CO_2 systems, whereas this parameter is completely bound to the pump inlet temperature in SCARABEUS ones, due to the condensing nature of these cycles; on the other hand, the latter present an added degree of freedom, which is the possibility to optimise the composition of the blend, hence directly modifying the critical conditions of the working fluid, enabling its condensation even at high ambient temperatures. This happens to be of uttermost importance, since one of the key-factors of the outstanding thermal performance presented by sCO_2 technology is its extremely low compression work, enabled by a low compressibility factor. Nevertheless, this is only valid if the compression process is operated in the extreme vicinity of the critical point, since the compressibility factor significantly increases as long as the main compressor inlet is shifted away from this particular condition. Bearing all this in mind, it is clear that pure CO_2 cycles do not present any means to avoid the strong rise in $\bar{Z}$ in high ambient temperature scenarios, and the consequent increase in compression work. As a consequence, cycle thermal performance is maximised reducing the main compressor pressure ratio – increasing main compressor inlet pressure, even at the cost of decreasing cycle specific work – with the purpose of increasing turbine outlet temperature in order to enhance the heat recuperation potential of the cycle. This can be better understood observing the relative deviations of $\bar{Z}$, W_s and ΔT_{PHX} in Fig. 15. Furthermore, it can be noticed that the difference between the exergy efficiency of RC CO_2 and PC CO_2 decreases significantly with the minimum cycle temperature (see Fig. 14, passing from 1.5pp at 35 °C to less than 0.2pp at 60 °C). This is brought by the different strategies employed by this configurations to maximise their thermal performance, and it can also be inferred from Fig. 15: PC CO_2 exhibits a reduction in the main compressor pressure ratio higher than the one of RC CO_2, but a lower reduction in the turbine expansion ratio. This is due to the fact that PC

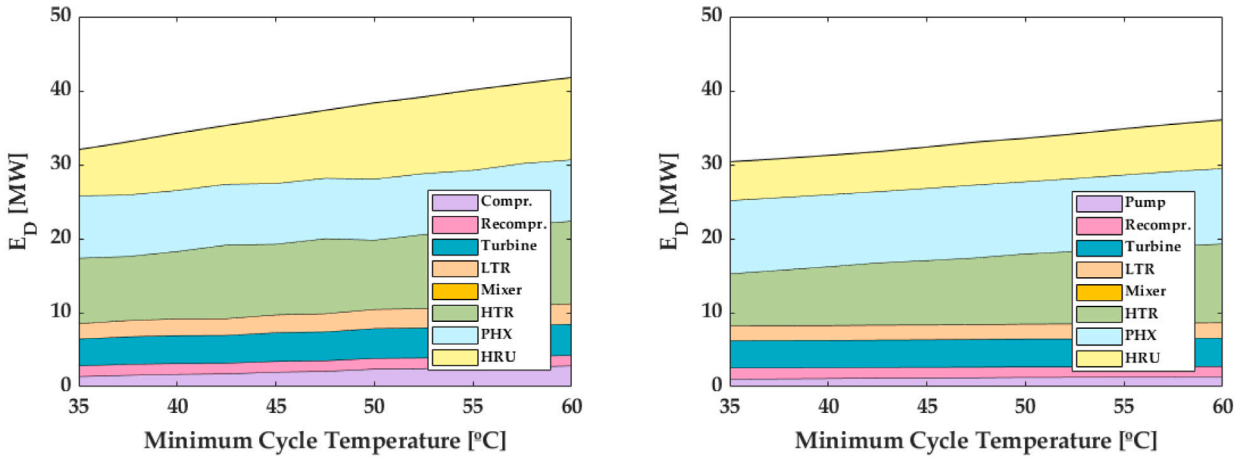

(**a**) *Recompression* with sCO_2 (**b**) *Recompression* with $\%CO_2$-$\%SO_2$ blend

Fig. 16. Exergy destruction breakdown as a function of design minimum cycle temperature. *Recompression* cycle with pure CO_2 (a) and CO_2-SO_2 blend (b).

CO_2 cycle overcomes the constraint imposed by the main compressor inlet pressure on the turbine exhaust – thanks to the addition of a precompressor (see Section 2) – and ER_{turb} can be optimised to face the rise in T_{min}. As a consequence, PC CO_2 achieves exergy efficiency similar to the one obtained by RC CO_2, but with greater specific work (i.e. lower circulating mass flow, smaller footprint) and higher ΔT_{PHX} (smaller size and, expectedly, cost of the TES). This fact results to be of utmost importance, as it affirms the *Partial Cooling* as the most promising pure CO_2 cycle configuration for high ambient temperatures, also from a techno-economic standpoint.

With regards to the blended systems, the main reason behind the superiority of SCARABEUS concept at high T_{min} (see Fig. 14) is the condensing nature of these cycles, which allows the pump to operate with a low mean compressibility factor even at extreme ambient conditions. As it can be observed in Fig. 15, SCARABEUS systems show a limited rise in $\bar{Z}$, in the order of 15%, whilst this parameter grows by more than 35% in RC CO_2 and PC CO_2. In spite of this, the three SCARABEUS systems present relative reductions of specific work ranging 25%–40%, values comparable to, or even higher than, the ones observed for pure sCO_2 cycles. This leads to a scenario in which cycle pressure ratio is also decreasing, due to two counteracting effects: first and foremost, for a given blend composition, working fluid condensing pressure (i.e. pump inlet pressure) always increases with bubble temperature (i.e. minimum cycle temperature, see Fig. 2); secondly, and to a smaller extent, a rise in dopant molar fraction leads to a decrease in the condensing pressure, for a given bubble temperature [24,35]. As a consequence, increasing the molar fraction of dopant (i.e. *tailor* the working fluid composition) appears to be a possible means of mitigating the drop in the cycle pressure ratio caused by the increase in minimum cycle temperature, hence increasing cycle performance. This *tailorability* can be defined as the ability to adjust the properties of the fluid to variations in the design T_{min} in order to best exploit the characteristics of the thermodynamic cycle employed. In this regard, the optimum dopant molar fraction for each SCARABEUS system is shown in Fig. 14 by means of different colour scales, being a darker colour representative of a higher molar fraction (for a given dopant). Furthermore, the value of the resulting optimum molar fraction is also indicated by labels, in order to improve figure readability. It can be observed that the dopant molar fraction increases with T_{min} when Hexafluorobenze (PrC D1) and Sulfur Dioxide (RC D3) are considered (from 12% to 17% and from 16% to 28% respectively), whereas for it presents a very slight reduction if Titanium Tetrachloride is taken into account (RR D2). This indicates a somehow better working fluid tailorability for PrC D1 and RC D3 systems in comparison with RR D2 one, which is also consistent with the less steep trends exhibited by the former cycle configurations (see Fig. 14). Bearing all this in mind, the significant reduction in W_s experimented by RR D2 (observed in Fig. 15) can be explained by its low tailorability, together with the extremely recuperative nature of this system, already discussed in Section 4.1. In this regard, the tendency towards lower molar fraction follows a rationale similar to the one previously discussed for pure CO_2 systems: in order to optimise thermal efficiency, the heat recuperation potential is significantly enhanced (see the vast reduction in ΔT_{PHX} in Fig. 15), at the expense of its specific work. On the contrary, the advanced layout configurations of PrC D1 and RC D3, together with their good tailorability, allows a better compromise between heat recuperation and specific work. This fact results to be more accentuated for the Precompression cycle with C_6F_6, due to the possibility of optimise the expansion ratio of the turbine independently, brought by the addition of a precompressor between the low and high temperature recuperators (see Sections 2 and 4.1).

Finally, Fig. 16 compares the exergy destruction breakdown of the *Recompression* cycle working on pure CO_2 (a) and on CO_2-SO_2 mixture (b), in order to better describe the effects of the change in working fluid for a given layout. The major difference is found in the growth of exergy destruction of the HRU with T_{min}. For the RC CO_2, it changes from 6.22 to 11.09 MW (+78%) whereas for RC D3 5.20 to 6.53 MW (+26%). This larger irreversibilities in the sCO_2 case is brought by a higher temperature rise in the compression process (see ΔT_{compr} in Fig. 15) which ultimately lead to an increase in the HRU inlet temperature. The remaining components are just responsible of a 4.9 MW (+19%) and 4.3 MW (+17%) increment, respectively.

5. Conclusions

The aim of this work is to explore the 2nd Law performance of transcritical power cycles working on blended Carbon Dioxide in order to assess their actual potential and the reasons for the expected performance gains with respect to either contemporary steam turbine technology or pure supercritical CO_2 cycles. To this end, the paper has presented a thorough comparison of three CSP power cycle technologies (steam Rankine, pure sCO_2 and blended sCO_2) based on exergy analysis for two different turbine inlet temperatures (550 and 700 °C) and one single minimum cycle temperature (50 °C). Three different candidate additive has been considered, namely Hexafluorobenzene (C_6F_6), Titanium Tetrachloride ($TiCl_4$) and Sulfur Dioxide (SO_2). A series of interesting conclusions can be drawn, putting this technology forward as a very promising alternative for mid-term future of CSP plant:

- The large temperature glide of CO_2-C_6F_6 and, especially, CO_2-$TiCl_4$ mixtures leads to working fluid condensation inside the recuperator, being this feature the main driver of the large cycle efficiency achieved by these two fluids with a *Recuperated Rankine* cycle.
- On the contrary, the lack of internal condensation observed with CO_2-SO_2 mixtures results to be extremely beneficial for the adoption of a *Recompression* layout.
- sCO_2 blends are a promising working fluid even at turbine inlet temperatures as low as 550 °C, enabling better energy and exergy efficiencies than state-of-the-art steam Rankine (1.8 and 2.7 pp higher 1st and 2nd Law efficiencies, respectively);
- At 700 °C, sCO_2 mixtures clearly outperform both state-of-the-art (steam) Rankine cycles and pure sCO_2 cycles, achieving thermal and exergy efficiencies as high as 51.6 and 75.3%. This confirms that the technology is a firm candidate for next generations CSP plants;
- Compared to pure sCO_2 cycles, using sCO_2 mixtures leads to a significant drop in the amount of exergy destroyed across the compression and heat rejection processes, rounding 50% for a given cycle output. This is enabled by the possibility to condense the working fluid. On the other hand, a larger (relative) E_D is experienced in the recuperators, even if this is still comparable to pure sCO_2 cycles from a quantitative standpoint. This sets a focus area for future research of CO_2 mixtures, where solutions to tackle the larger irreversibilities of these components will have to be devised;
- The interest in considering maximum cycle pressures higher that 250 bar is extremely scarce, due to the very limited gains achieved in thermal performance. For a *Precompression* cycle operated with CO_2-C_6F_6 blends, this threshold value can be reduced to 200 bar;
- At high ambient temperatures, CO_2 mixtures behave significantly better than pure CO_2. The gain, in terms of exergy efficiency, can be as high as 3 percentage points, for a minimum cycle temperature of 60 °C;
- This enhanced performance achieved by CO_2 mixtures is brought by the condensing nature of the cycle, together with the tailorability of the working fluid (i.e. possibility to optimise the molar fraction of dopant as a function of minimum cycle temperature, in order to maximise cycle thermal efficiency).

Declaration of competing interest

The authors declare that they have no known competing financial interests or personal relationships that could have appeared to influence the work reported in this paper.

Acknowledgements

The SCARABEUS project has received funding from the European Union's Horizon 2020 research and innovation programme under grant agreement Nº814985. The University of Seville is also gratefully acknowledged for supporting this research through its Internal Research Programme (Plan Propio de Investigación), under contract No 2019/00000359. Last but not least, the regional government of Andalusia (Junta de Andalucía) is gratefully acknowledged for sponsoring the contract of Pablo Rodríguez de Arriba under the Programme for Youth Employment 2014–2020 (Phase 4).

Appendix. Complete heat & mass balances and resume of exergy balances by components

This annex presents the complete heat & mass balances and a resume of exergy balances by components for all the CO_2-based systems considered in the present paper (see Tables A.8–A.17). The entire set of cycles have been optimised following the methodology discussed in Section 4.1. The results refer to two different turbine inlet temperature levels, 550 °C and 700 °C. The flow exergy of each cycle station (E) have been expressed taking as reference the exergy at cycle station 1 (E_1=0), for each combination of cycle layout/TIT. In this regard, cycle stations refers to Fig. 1.

Table A.8
Heat & mass balance of *Recompression* cycle with pure CO_2. Two temperature levels are considered, cycle stations refers to Fig. 1a.

	Cycle stations	T [°C]	P [bar]	$\dot{m}$ [kg/s]	h [kJ/kg]	s [kJ/kg K]	E [kJ/kg]	ρ [kg/m^3]	Z [-]
TIT=550 °C	1	50.0	105.3	999.1	367.0	1.52	0.0	450.0	0.38
	2	96.7	250.0	999.1	397.0	1.53	27.0	604.0	0.59
	3	182.9	246.3	999.1	558.0	1.93	64.0	346.0	0.83
	4	182.9	246.3	1407.2	558.0	1.93	64.0	346.0	0.83
	5	417.1	242.7	1407.2	867.0	2.48	200.0	183.0	1.02
	6	550.0	239.1	1407.2	1032.0	2.70	296.0	147.0	1.04
	7	451.1	108.5	1407.2	923.0	2.71	183.0	79.0	1.01
	8	187.9	107.5	1407.2	615.0	2.19	40.0	137.0	0.90
	9	101.7	106.4	1407.2	502.0	1.91	12.0	203.0	0.74
	10	182.9	246.3	408.1	558.0	1.93	64.0	346.0	0.83
TIT=700 °C	1	50.0	102.2	752.1	377.0	1.55	0.0	412.0	0.41
	2	102.3	250.0	752.1	409.0	1.56	29.6	578.0	0.61
	3	193.4	246.3	752.1	574.0	1.96	69.8	330.0	0.85
	4	193.4	246.3	1059.3	574.0	1.96	69.8	330.0	0.85
	5	549.5	242.7	1059.3	1032.0	2.70	296.7	150.0	1.04
	6	700.0	239.1	1059.3	1222.0	2.91	419.6	123.0	1.05
	7	586.1	105.3	1059.3	1086.0	2.93	280.3	64.0	1.02
	8	198.4	104.3	1059.3	629.0	2.22	43.5	128.0	0.91
	9	107.3	103.3	1059.3	513.0	1.95	12.8	188.0	0.77
	10	193.3	246.3	307.2	574.0	1.96	69.8	330.0	0.85

Table A.9
Resume of exergy balance by components. The results, expressed in MW, refers to *Recompression* cycle with pure CO_2. Two temperature levels are considered, cycle stations refers to Fig. 1a.

Cycle components	Cycle stations	TIT = 550 °C					TIT = 700 °C				
		E_F	E_P	E_L	E_D	ϵ_k [%]	E_F	E_P	E_L	E_D	ϵ_k [%]
Compressor	1–2	30.06	27.26	0.00	2.81	90.67	24.55	22.29	0.00	2.26	90.80
Recompressor	9–10	23.17	21.41	0.00	1.76	92.41	18.91	17.50	0.00	1.40	92.58
Turbine	6–7	158.43	153.41	0.00	5.02	96.83	147.51	143.55	0.00	3.96	97.32
Low temp. recuperator	2–3/8–9	39.87	37.02	0.00	2.85	92.85	32.50	30.20	0.00	2.30	92.91
Mixer	3–4–10	90.52	90.52	0.00	0.00	100.00	73.91	73.91	0.00	0.00	100.00
High temp. recuperator	4–5/7–8	201.50	190.63	0.00	10.87	94.61	250.90	240.38	0.00	10.51	95.81
Primary heat exchanger	5–6	147.25	135.31	0.00	11.94	91.89	138.35	130.16	0.00	8.19	94.08
Heat rejection unit	9–1	11.84	0.00	0.00	11.84	–	9.62	0.00	0.00	9.62	–

Table A.10
Heat & mass balance of *Partial Cooling* cycle with pure CO_2. Two temperature levels are considered, cycle stations refers to Fig. 1b.

	Cycle stations	T [°C]	P [bar]	$\dot{m}$ [kg/s]	h [kJ/kg]	s [kJ/kg K]	E [kJ/kg]	ρ [kg/m^3]	Z [-]
TIT=550 °C	1	50.0	112.2	604.8	349.0	1.46	0.0	524.0	0.35
	2	87.0	250.0	604.8	375.0	1.47	23.4	651.0	0.56
	3	156.2	246.3	604.8	515.0	1.83	51.0	395.0	0.77
	4	156.2	246.3	1008.0	515.0	1.83	50.9	395.0	0.77
	5	360.9	242.7	1008.0	797.0	2.37	162.0	203.0	1.00
	6	550.0	239.1	1008.0	1032.0	2.70	295.1	147.0	1.04
	7	409.2	75.3	1008.0	879.0	2.72	136.1	58.0	1.00
	8	161.2	74.5	1008.0	598.0	2.21	14.6	100.0	0.90
	9	92.0	73.8	1008.0	514.0	2.00	−3.8	133.0	0.80
	10	50.0	73.0	1008.0	449.0	1.81	−9.7	185.0	0.65
	11	86.9	113.3	1008.0	470.0	1.82	9.0	251.0	0.66
	12	156.2	246.3	403.2	515.0	1.83	50.9	395.0	0.77
TIT=700 °C	1	50.0	111.5	423.7	351.0	1.47	0.0	518.0	0.35
	2	87.7	250.0	423.7	377.0	1.48	23.7	647.0	0.57
	3	175.6	246.3	423.7	547.0	1.90	60.1	358.0	0.81
	4	175.6	246.3	718.2	547.0	1.90	60.1	358.0	0.81
	5	474.9	242.7	718.2	938.0	2.58	239.6	166.0	1.03
	6	700.0	239.1	718.2	1222.0	2.91	418.4	123.0	1.05
	7	524.5	64.7	718.2	1016.0	2.93	205.9	43.0	1.01
	8	180.6	64.0	718.2	624.0	2.30	14.1	80.0	0.93
	9	92.7	63.4	718.2	523.0	2.05	−9.7	110.0	0.83
	10	50.0	62.8	718.2	465.0	1.88	−15.3	145.0	0.71
	11	101.1	112.7	718.2	495.0	1.89	12.6	220.0	0.72
	12	175.6	246.3	294.4	547.0	1.90	60.1	358.0	0.81

Table A.11
Resume of exergy balance by components. The results, expressed in MW, refers to *Partial Cooling* cycle with pure CO_2. Two temperature levels are considered, cycle stations refers to Fig. 1b.

Cycle components	Cycle stations	TIT = 550 °C					TIT = 700 °C				
		E_F	E_P	E_L	E_D	ϵ_k [%]	E_F	E_P	E_L	E_D	ϵ_k [%]
Compressor	1–2	15.63	14.13	0.00	1.50	90.42	11.09	10.03	0.00	1.06	90.44
Recompressor	11–12	18.40	16.92	0.00	1.48	91.95	15.15	13.98	0.00	1.17	92.29
Precompressor	10–11	20.85	18.85	0.00	2.00	90.42	22.05	20.01	0.00	2.03	90.77
Turbine	6–7	160.34	154.95	0.00	5.39	96.64	152.65	148.23	0.00	4.42	97.11
Low temp. recuperator	2–3/8–9	18.46	16.68	0.00	1.77	90.39	17.13	15.43	0.00	1.70	90.08
Mixer	3–4–12	51.36	51.36	0.00	0.00	100.00	43.15	43.15	0.00	0.00	100.00
High temp. recuperator	4–5/7–8	122.47	111.98	0.00	10.49	91.44	137.71	128.93	0.00	8.78	93.62
Primary heat exchanger	5–6	150.05	134.15	0.00	15.90	89.40	139.70	128.44	0.00	11.26	91.94
Heat rejection unit ♯ 1	9–10	6.02	0.00	0.00	6.02	–	4.00	0.00	0.00	4.00	–
Heat rejection unit ♯ 2	11–1	5.43	0.00	–	5.43	0.00	5.34	0.00	0.00	5.34	–

Table A.12
Heat & mass balance of *Precompression* cycle with 85%CO_2–15%C_6F_6. Two temperature levels are considered, cycle stations refers to Fig. 1d.

	Cycle stations	T [°C]	P [bar]	$\dot{m}$ [kg/s]	h [kJ/kg]	s [kJ/kg K]	E [kJ/kg]	ρ [kg/m^3]	Z [-]
TIT=550 °C	1	50.0	77.8	1152.8	−7488.0	−1.48	0.0	894.0	0.21
	2	71.1	250.0	1152.8	−7468.0	−1.47	18.0	1004.0	0.57
	3	211.0	246.3	1152.8	−7238.0	−0.91	72.0	495.0	0.81
	4	401.5	242.7	1152.8	−6973.0	−0.44	191.0	281.0	1.00
	5	550.0	239.1	1152.8	−6774.0	−0.17	306.0	217.0	1.05
	6	437.7	61.1	1152.8	−6898.0	−0.16	178.0	68.0	0.99
	7	215.9	60.5	1152.8	−7163.0	−0.60	52.0	108.0	0.90
	8	237.3	79.3	1152.8	−7146.0	−0.60	68.0	136.0	0.89
	9	87.2	78.5	1152.8	−7376.0	−1.15	8.0	309.0	0.55
TIT=700 °C	1	50.0	77.8	878.5	−7488.0	−1.48	0.0	894.0	0.21
	2	71.1	250.0	878.5	−7468.0	−1.47	18.2	1004.0	0.57
	3	237.9	246.3	878.5	−7198.0	−0.83	86.8	444.0	0.85
	4	534.0	242.7	878.5	−6796.0	−0.20	293.4	225.0	1.05
	5	700.0	239.1	878.5	−6570.0	0.06	439.0	180.0	1.07
	6	572.3	56.9	878.5	−6728.0	0.07	276.3	52.0	1.01
	7	242.9	56.3	878.5	−7130.0	−0.53	61.7	93.0	0.92
	8	270.4	79.3	878.5	−7106.0	−0.53	84.2	124.0	0.92
	9	87.1	78.5	878.5	−7376.0	−1.15	8.4	309.0	0.55

Table A.13
Resume of exergy balance by components. The results, expressed in MW, refers to *Precompression* cycle with pure 85%CO_2–15%C_6F_6. Two temperature levels are considered, cycle stations refers to Fig. 1d.

Cycle components	Cycle stations	TIT = 550 °C					TIT = 700 °C				
		E_F	E_P	E_L	E_D	ϵ_k [%]	E_F	E_P	E_L	E_D	ϵ_k [%]
Pump	1–2	23.59	21.01	0.00	2.57	89.09	17.98	16.02	0.00	1.96	89.09
Precompressor	7–8	19.93	18.58	0.00	1.34	93.25	21.02	19.69	0.00	1.34	93.64
Turbine	4–5	148.30	143.52	0.00	4.79	96.77	142.90	139.00	0.00	3.90	97.27
Low temp. recuperator	2–3/8–9	68.72	61.95	0.00	6.77	90.14	66.59	60.21	0.00	6.38	90.41
High temp. recuperator	3–4/6–7	144.87	137.62	0.00	7.25	95.00	188.52	181.53	0.00	6.98	96.30
Primary heat exchanger	4–5	144.59	132.37	0.00	12.23	91.54	136.19	127.91	0.00	8.28	93.92
Heat rejection unit	9–1	9.64	0.00	0.00	9.64	–	7.34	0.00	0.00	7.34	–

Table A.14
Heat & mass balance of *Recuperated Rankine* cycle with 83%CO_2–17%$TiCl_4$. Two temperature levels are considered, cycle stations refers to Fig. 1c.

	Cycle stations	T [°C]	P [bar]	$\dot{m}$ [kg/s]	h [kJ/kg]	s [kJ/kg K]	E [kJ/kg]	ρ [kg/m^3]	Z [-]
TIT=550 °C	1	50.0	96.2	1575.3	−6837.0	−1.22	0.0	1129.0	0.22
	2	63.4	250.0	1575.3	−6822.0	−1.22	13.0	1189.0	0.52
	3	411.7	246.3	1575.3	−6376.0	−0.28	167.0	303.0	0.98
	4	550.0	242.7	1575.3	−6237.0	−0.10	247.0	236.0	1.04
	5	449.6	98.1	1575.3	−6316.0	−0.09	166.0	114.0	0.98
	6	71.9	97.1	1575.3	−6762.0	−1.00	4.0	490.0	0.48
TIT=700 °C	1	50.0	96.2	1239.9	−6837.0	−1.22	0.0	1129.0	0.22
	2	63.4	250.0	1239.9	−6822.0	−1.22	13.4	1189.0	0.52
	3	541.3	246.3	1239.9	−6246.0	−0.11	242.2	242.0	1.03
	4	700.0	242.7	1239.9	−6090.0	0.07	343.0	195.0	1.06
	5	589.3	98.1	1239.9	−6185.0	0.08	244.6	93.0	1.01
	6	71.9	97.1	1239.9	−6762.0	−1.00	4.2	490.0	0.48

Table A.15
Resume of exergy balance by components. The results, expressed in MW, refers to *Recuperated Rankine* cycle with pure 83%CO_2–17%$TiCl_4$. Two temperature levels are considered, cycle stations refers to Fig. 1c.

Cycle components	Cycle stations	TIT = 550 °C					TIT = 700 °C				
		E_F	E_P	E_L	E_D	ϵ_k [%]	E_F	E_P	E_L	E_D	ϵ_k [%]
Pump	1–2	23.76	21.14	0.00	2.62	88.97	18.70	16.64	0.00	2.06	88.97
Turbine	4–5	127.82	123.76	0.00	4.06	96.83	121.97	118.70	0.00	3.26	97.32
Heat recuperator	2-3/5–6	254.95	241.44	0.00	13.50	94.70	298.10	283.72	0.00	14.39	95.17
Primary heat exchanger	3–4	138.08	126.77	0.00	11.31	91.81	132.93	124.91	0.00	8.02	93.97
Heat rejection unit	6–1	6.59	0.00	0.00	6.59	–	5.20	0.00	0.00	5.20	–

Table A.16
Heat & mass balance of *Recompression* cycle with 80%CO_2–20%SO_2. Two temperature levels are considered, cycle stations refers to Fig. 1e.

	Cycle stations	T [°C]	P [bar]	$\dot{m}$ [kg/s]	h [kJ/kg]	s [kJ/kg K]	E [kJ/kg]	ρ [kg/m^3]	Z [-]
TIT=550 °C	1	50.0	79.1	665.3	−8008.0	−1.15	0.0	781.0	0.18
	2	74.3	250.0	665.3	−7984.0	−1.14	21.0	846.0	0.49
	3	187.3	246.3	665.3	−7763.0	−0.58	67.0	398.0	0.78
	4	187.4	246.3	1073.0	−7763.0	−0.58	67.0	398.0	0.78
	5	372.8	242.7	1073.0	−7524.0	−0.14	168.0	221.0	0.98
	6	550.0	239.1	1073.0	−7316.0	0.15	286.0	161.0	1.04
	7	415.4	81.5	1073.0	−7447.0	0.16	151.0	69.0	0.99
	8	192.3	80.7	1073.0	−7686.0	−0.26	43.0	113.0	0.89
	9	81.1	79.9	1073.0	−7824.0	−0.60	11.0	204.0	0.64
	10	187.4	246.3	407.8	−7763.0	−0.58	68.0	398.0	0.78
TIT=700 °C	1	50.0	79.1	512.8	−8008.0	−1.15	0.0	781.0	0.18
	2	74.3	250.0	512.8	−7984.0	−1.14	21.1	846.0	0.49
	3	187.3	246.3	512.8	−7763.0	−0.58	67.5	398.0	0.78
	4	187.3	246.3	827.1	−7763.0	−0.58	67.5	398.0	0.78
	5	499.3	242.7	827.1	−7376.0	0.07	250.9	176.0	1.03
	6	700.0	239.1	827.1	−7140.0	0.34	400.7	134.0	1.06
	7	550.6	81.5	827.1	−7299.0	0.36	237.6	57.0	1.01
	8	192.3	80.7	827.1	−7686.0	−0.26	42.6	113.0	0.89
	9	81.1	79.9	827.1	−7824.0	−0.60	11.3	204.0	0.64
	10	187.4	246.3	314.3	−7763.0	−0.58	67.5	398.0	0.78

Table A.17
Resume of exergy balance by components. The results, expressed in MW, refers to *Recompression* cycle with pure 80%CO_2–20%SO_2. Two temperature levels are considered, cycle stations refers to Fig. 1e.

Cycle components	Cycle stations	TIT = 550 °C					TIT = 700 °C				
		E_F	E_P	E_L	E_D	ϵ_k [%]	E_F	E_P	E_L	E_D	ϵ_k [%]
Pump	1–2	15.78	14.07	0.00	1.71	89.15	12.16	10.85	0.00	1.32	89.15
Recompressor	9–10	24.76	22.90	0.00	1.86	92.49	19.08	17.64	0.00	1.43	92.49
Turbine	6–7	145.30	140.46	0.00	4.84	96.67	134.95	131.17	0.00	3.78	97.20
Low temp. recuperator	2–3/8–9	33.56	30.82	0.00	2.74	91.84	25.87	23.76	0.00	2.12	91.82
Mixer	3–4–10	72.42	72.41	0.00	0.00	100.00	55.81	55.81	0.00	0.00	100.00
High temp. recuperator	4–5/7–8	116.07	108.18	0.00	7.90	93.20	161.22	151.73	0.00	9.49	94.12
Primary heat exchanger	5–6	140.63	126.52	0.00	14.11	89.97	133.65	123.88	0.00	9.77	92.69
Heat rejection unit	9–1	7.55	0.00	0.00	7.55	–	5.82	0.00	0.00	5.82	–

References

[1] F. Crespi, D. Sánchez, G.S. Martínez, T. Sánchez-Lencero, F. Jiménez-Espadafor, Potential of supercritical carbon dioxide power cycles to reduce the levelised cost of electricity of contemporary concentrated solar power plants, Appl. Sci. 10 (15) (2020) 5049, http://dx.doi.org/10.3390/app10155049.

[2] M.T. Islam, N. Huda, A. Abdullah, R. Saidur, A comprehensive review of state-of-the-art concentrating solar power (CSP) technologies: Current status and research trends, Renew. Sustain. Energy Rev. 91 (2018) 987–1018, http://dx.doi.org/10.1016/j.rser.2018.04.097, URL https://www.sciencedirect.com/science/article/pii/S1364032118303113.

[3] M. Mehos, C. Turchi, J. Vidal, M. Wagner, Z. Ma, C. Ho, W. Kolb, C. Andraka, A. Kruizenga, Concentrating Solar Power Gen3 Demonstration Roadmap, NREL/TP-5500-67464, National Renewable Energy Laboratory, Golden, Colorado, United States, 2017, p. 127, http://dx.doi.org/10.2172/1338899.

[4] C.S. Turchi, Z. Ma, T.W. Neises, M.J. Wagner, Thermodynamic study of advanced supercritical carbon dioxide power cycles for concentrating solar power systems, J. Sol. Energy Eng. 135 (4) (2013) 041007, http://dx.doi.org/10.1115/1.4024030.

[5] T. Neises, C. Turchi, Supercritical carbon dioxide power cycle design and configuration optimization to minimize levelized cost of energy of molten salt power towers operating at 650° c, Sol. Energy 181 (2019) 27–36, http://dx.doi.org/10.1016/j.solener.2019.01.078.

[6] F. Crespi, D. Sánchez, T. Sánchez, G.S. Martínez, Capital cost assessment of concentrated solar power plants based on supercritical carbon dioxide power cycles, J. Eng. Gas Turbines Power 141 (7) (2019) 071011, http://dx.doi.org/10.1115/1.4042304.

[7] J.-M. Yin, Q.-Y. Zheng, Z.-R. Peng, X.-R. Zhang, Review of supercritical CO_2 power cycles integrated with CSP, Int. J. Energy Res. 44 (3) (2020) 1337–1369, http://dx.doi.org/10.1002/er.4909.

[8] D. Thanganadar, F. Fornarelli, S. Camporeale, F. Asfand, J. Gillard, K. Patchigolla, Thermo-economic analysis, optimisation and systematic integration of supercritical carbon dioxide cycle with sensible heat thermal energy storage for CSP application, Energy 238 (2022) 121755, http://dx.doi.org/10.1016/j.energy.2021.121755.

[9] M.T. White, G. Bianchi, L. Chai, S.A. Tassou, A.I. Sayma, Review of supercritical CO_2 technologies and systems for power generation, Appl. Therm. Eng. 185 (2021) 116447, http://dx.doi.org/10.1016/j.applthermaleng.2020.116447.

[10] D. Kirk-Othmer, Encyclopedia of Chemical Technology, 4th edn., Vol. 23, Wiley Interscience Publication, 2001, http://dx.doi.org/10.1002/0471238961.

[11] G. Angelino, Perspectives for the liquid phase compression gas turbine, J. Eng. Power 89 (2) (1967) 229–236, http://dx.doi.org/10.1115/1.3616657.

[12] G. Angelino, Carbon dioxide condensation cycles for power production, J. Eng. Gas Turbines Power 90 (3) (1968) 287–295, http://dx.doi.org/10.1115/1.3609190.

[13] G. Angelino, Real gas effects in carbon dioxide cycles, in: ASME Gas Turbine Conference and Products Show, American Society of Mechanical Engineers, 1969, http://dx.doi.org/10.1115/69-GT-102.
[14] E.G. Feher, The supercritical thermodynamic power cycle, Energy Convers. 8 (2) (1968) 85–90.
[15] V. Dostal, A Supercritical Carbon Dioxide Cycle for Next Generation Nuclear Reactors (Ph.D. thesis), Massachusetts Institute of Technology, Department of Nuclear Engineering, 2004.
[16] F. Crespi, G. Gavagnin, D. Sánchez, G.S. Martínez, Supercritical carbon dioxide cycles for power generation: A review, Appl. Energy 195 (2017) 152–183, http://dx.doi.org/10.1016/j.apenergy.2017.02.048.
[17] K. Brun, P. Friedman, R. Dennis, Fundamentals and Applications of Supercritical Carbon Dioxide (SCO_2) Based Power Cycles, Woodhead Publishing, 2017.
[18] M.D. Carlson, B.M. Middleton, C.K. Ho, Techno-economic comparison of solar-driven sCO_2 brayton cycles using component cost models baselined with vendor data and estimates, in: Energy Sustainability, Vol. 57595, American Society of Mechanical Engineers, 2017, http://dx.doi.org/10.1115/ES2017-3590, V001T05A009.
[19] N.T. Weiland, B.W. Lance, S.R. Pidaparti, SCO_2 power cycle component cost correlations from DOE data spanning multiple scales and applications, in: ASME Turbo Expo: Turbomachinery Technical Conference and Exposition, 2019, http://dx.doi.org/10.1115/GT2019-90493, American Society of Mechanical Engineers Digital Collection.
[20] C.S. Turchi, M. Boyd, D. Kesseli, P. Kurup, M.S. Mehos, T.W. Neises, P. Sharan, M.J. Wagner, T. Wendelin, CSP Systems Analysis - Final Project Report, NREL/TP-5500-72856, National Renewable Energy Laboratory, Golden, Colorado, United States, 2019, p. 87, http://dx.doi.org/10.2172/1513197.
[21] M. Mehos, C. Turchi, J. Jorgenson, P. Denholm, C. Ho, K. Armijo, On the Path to SunShot - Advancing Concentrating Solar Power Technology, Performance, and Dispatchability, NREL/TP-5500-65688 SAND-2016-2237 R 7620, EERE Publication and Product Library, Washington, D.C. (United States, 2016, p. 51, http://dx.doi.org/10.2172/1344199.
[22] Energy.gov, 2030 Solar cost targets, 2021, URL https://www.energy.gov/eere/solar/articles/2030-solar-cost-targets, Online, accessed May 26th 2022.
[23] D. Alfani, T. Neises, M. Astolfi, M. Binotti, P. Silva, Techno-economic analysis of CSP incorporating sCO_2 brayton power cycles: Trade-off between cost and performance, AIP Conf. Proc. 2445 (1) (2022) 090001, http://dx.doi.org/10.1063/5.0086353.
[24] F. Crespi, P. Rodríguez de Arriba, D. Sánchez, A. Ayub, G. Di Marcoberardino, C.M. Invernizzi, G.S. Martínez, P. Iora, D. Di Bona, M. Binotti, et al., Thermal efficiency gains enabled by using CO_2 mixtures in supercritical power cycles, Energy 238 (2022) 121899, http://dx.doi.org/10.1016/j.energy.2021.121899.
[25] C.M. Invernizzi, T. van der Stelt, Supercritical and real gas brayton cycles operating with mixtures of carbon dioxide and hydrocarbons, Proc. Inst. Mech. Eng., Part A: J. Power Energy 226 (5) (2012) 682–693, http://dx.doi.org/10.1177/0957650912444689.
[26] C.M. Invernizzi, Prospects of mixtures as working fluids in real-gas brayton cycles, Energies 10 (10) (2017) 1649, http://dx.doi.org/10.3390/en10101649.
[27] S. Baik, J.I. Lee, Preliminary study of supercritical CO_2 mixed with gases for power cycle in warm environments, in: Turbo Expo: Power for Land, Sea, and Air, Vol. 51180, American Society of Mechanical Engineers, 2018, http://dx.doi.org/10.1115/GT2018-76386, V009T38A017.
[28] G. Manzolini, M. Binotti, D. Bonalumi, M.C. Invernizzi, P. Iora, CO_2 mixtures as innovative working fluid in power cycles applied to solar plants. Techno-economic assessment, Sol. Energy 181 (2019) 530–544, http://dx.doi.org/10.1016/j.solener.2019.01.015.
[29] R. Valencia-Chapi, L. Coco-Enríquez, J. Muñoz-Antón, Supercritical CO_2 mixtures for advanced brayton power cycles in line-focusing solar power plants, Appl. Sci. 10 (1) (2020) 55, http://dx.doi.org/10.3390/app10010055.
[30] R. Valencia-Chapi, L. Coco-Enríquez, J. Muñoz-Antón, Comparing line-focusing and central tower solar power plants with s-CO_2 binary mixture brayton power cycles, in: AIP Conference Proceedings, Vol. 2303, (1) AIP Publishing LLC, 2020, 130010, http://dx.doi.org/10.1063/5.0028661.
[31] Supercritical CARbon dioxide/alternative fluids blends for efficiency upgrade of solar power plants, 2019, URL https://cordis.europa.eu/project/rcn/221766/factsheet/en, Online, accessed May 12th 2021.
[32] R.V. Padilla, Y.C.S. Too, R. Benito, W. Stein, Exergetic analysis of supercritical CO_2 brayton cycles integrated with solar central receivers, Appl. Energy 148 (2015) 348–365, http://dx.doi.org/10.1016/j.apenergy.2015.03.090.
[33] M. Penkuhn, G. Tsatsaronis, Systematic evaluation of efficiency improvement options for sCO_2 brayton cycles, Energy 210 (2020) 118476, http://dx.doi.org/10.1016/j.energy.2020.118476.
[34] F. Crespi, G.S. Martínez, P. Rodriguez de Arriba, D. Sánchez, F. Jiménez-Espadafor, Influence of working fluid composition on the optimum characteristics of blended supercritical carbon dioxide cycles, in: Turbo Expo: Power for Land, Sea, and Air, Vol. 85048, American Society of Mechanical Engineers, 2021, http://dx.doi.org/10.1115/GT2021-60293, V010T30A030.
[35] F. Crespi, P. Rodríguez de Arriba, D. Sánchez, A. Muñoz, Preliminary investigation on the adoption of CO_2-SO_2 working mixtures in a transcritical recompression cycle, Appl. Therm. Eng. 211 (2022) 118384, http://dx.doi.org/10.1016/j.applthermaleng.2022.118384.
[36] Rice solar, 2021. Rice solar energy project, URL https://www.wapa.gov/transmission/interconnection/Pages/rice-solar.aspx, Retrieved January 1st 2022.
[37] NFPA 704: Standard system for the identification of the hazards of materials for emergency response, URL https://www.nfpa.org/codes-and-standards/all-codes-and-standards/list-of-codes-and-standards/detail?code=704, Retrieved January 1st 2022.
[38] Aspen Tecnology Inc., 2022. Aspen Plus v9 - Leading process simulator software, URL https://www.aspentech.com/en/products/engineering/aspen-properties, Retrieved January 1st 2022.
[39] Thermoflow Inc., 2021. Thermoflow suite - Thermoflex software v.29, URL https://www.thermoflow.com/products_generalpurpose.html, Retrieved January 1st 2022.
[40] E. Lemmon, I.H. Bell, M. Huber, M. McLinden, NIST standard reference database 23: Reference fluid thermodynamic and transport properties-REFPROP, version 10.0, national institute of standards and technology, Stand. Ref. Data Program, Gaithersburg (2018).
[41] D. Bonalumi, S. Lasala, E. Macchi, CO_2-$ticl_4$ working fluid for high-temperature heat source power cycles and solar application, Renew. Energy 147 (2020) 2842–2854, http://dx.doi.org/10.1016/j.renene.2018.10.018.
[42] W.C. Reynolds, P. Colonna, Thermodynamics: Fundamentals and Engineering Applications, Cambridge University Press, 2018, http://dx.doi.org/10.1017/9781139050616.
[43] G. Tsatsaronis, Definitions and nomenclature in exergy analysis and exergoeconomics, Energy 32 (4) (2007) 249–253, http://dx.doi.org/10.1016/j.energy.2006.07.002.
[44] A. Bejan, G. Tsatsaronis, M.J. Moran, Thermal Design and Optimization, John Wiley & Sons, 1995.
[45] D. Novales, A. Erkoreka, V. De la Peña, B. Herrazti, Sensitivity analysis of supercritical CO_2 power cycle energy and exergy efficiencies regarding cycle component efficiencies for concentrating solar power, Energy Convers. Manage. 182 (2019) 430–450, http://dx.doi.org/10.1016/j.enconman.2018.12.016.
[46] C.M. Invernizzi, Closed Power Cycles: Thermodynamic Fundamentals and Applications, Vol. 11, Springer Science & Business Media, 2013.
[47] F. Crespi, G. Gavagnin, D. Sánchez, G.S. Martínez, Analysis of the thermodynamic potential of supercritical carbon dioxide cycles: A systematic approach, J. Eng. Gas Turbines Power 140 (5) (2017) 051701, http://dx.doi.org/10.1115/1.4038125.
[48] D. Sánchez, F. Crespi, P. Rodríguez de Arriba, A. Muñoz, G. Manzolini, C. Invernizzi, G. Di Marcoberardino, M. White, P. David, Potential and challenges of the utilization of CO_2-mixtures in supercritical power cycles of concentrated solar power plants, in: Proceedings of the Supercritical CO_2 Power Cycles Symposium, 2022, URL https://sco2symposium.com/proceedings.shtml.